Adapting the thermal-based two-source energy balance model to estimate daytime turbulent fluxes in a complex tree-grass ecosystem

Vicente Burchard-Levine[1]*, Héctor Nieto[2], David Riaño[1, 3], Mirco Migliavacca[4], Tarek S. El-Madany[4], Oscar Perez-Priego[5], Arnaud Carrara[6] and M. Pilar Martín[1]

[1] Environmental Remote Sensing and Spectroscopy Laboratory (SpecLab), Spanish National Research Council (CSIC), Madrid, Spain; vicentefelipe.burchard@cchs.csic.es; mpilar.martin@cchs.csic.es; david.riano@cchs.csic.es
[2] Complutum Tecnologías de la Información Geográfica S.L. (COMPLUTIG), Alcalá de Henares, Spain. hector.nieto@complutig.com
[3] Center for Spatial Technologies and Remote Sensing (CSTARS), University of California, 139 Veihmeyer Hall, One Shields Avenue, Davis, CA 95616,USA
[4] Max Planck Institute for Biogeochemistry, Department Biogeochemical Integration, Hans-Knöll-Str. 10, 07745 Jena, Germany; mmiglia@bgc-jena.mpg.de; telmad@bgc-jena.mpg.de
[5] Department of Biological Sciences, Macquarie University, Sydney, NSW, 2109, Australia; oscar.perez-priego@mq.edu.au
[6] Fundación Centro de Estudios Ambientales del Mediterráneo (CEAM), Valencia 46980, Spain; arnaud@ceam.es

Correspondence to: Vicente Burchard-Levine (vicentefelipe.burchard@cchs.csic.es)

Abstract. The thermal-based Two-Source Energy Balance (TSEB) model has accurately simulated energy fluxes in a wide range of landscapes. However, tree-grass ecosystems (TGE) have notably complex heterogenous vegetation mixtures and dynamic phenological characteristics presenting clear challenges to earth observation and modeling methods. The TSEB model was tested in a TGE ecosystem and an adaptation was proposed to consider spatial and temporal complexity. This was based on sensitivity analyses (SA) conducted on both primary remote sensing inputs (local SA) and model parameters (global SA). The model was subsequently modified taking into account phenological dynamics and assuming a dominant vegetation structure and cover (i.e. either grassland or broadleaved trees) for different seasons (TSEB-2S). The adaptation was compared against the default (i.e. non-seasonally changing) model and evaluated against eddy covariance (EC) flux measurements and lysimeters over a TGE experimental site in central Spain. TSEB-2S vastly improved over the default TSEB performance decreasing the mean bias and RMSD of LE from 34 and 77 W m^{-2} to 0 and 59 W m^{-2}, respectively during 2015. TSEB-2S was further validated for two other EC towers and for different years (2015, 2016 and 2017) obtaining similar error statistics with RMSE of LE ranging between 51 and 63 W m^{-2}. The results presented here demonstrate the important role that vegetation, through its structure and phenology, has in controlling ecosystem level energy fluxes, which become important considerations for the modeling procedure. Additionally, TSEB was shown to be most sensitive to parameters related to radiation partitioning between canopy and soil, such as characterizing vegetation clumping, and parameters related to vegetation structure involved in quantifying the resistance to turbulent flow.

List of Acronyms

Variable	Description	Units
α_{PT}	*Priestley Taylor coefficient for potential transpiration*	-
b	*Soil-surface resistance (Rs) constant*	-
c	*Constant in soil-surface resistance (Rs)*	m s^{-1} $K^{-1/3}$
C'	*Constant in total boundary resistance (Rx)*	$s^{1/2}$ m^{-1}
c_d	*Equivalent drag coefficient of the foliage elements*	-
f_c	*Fractional cover*	-
f_g	*Fraction of vegetation that is green*	-
G	*Soil heat flux*	W m^{-2}
h_c	*Canopy height*	m
H	*Sensible heat flux*	W m^{-2}
H_c	*Sensible heat flux from canopy source*	W m^{-2}
H_s	*Sensible heat flux from soil source*	W m^{-2}
k_{be}	*Beam extinction coefficient*	-
LAI	*Leaf Area Index*	m^2 m^{-2}
LE	*Latent heat flux*	W m^{-2}
LE_c	*Latent heat flux from the canopy source*	W m^{-2}
LE_s	*Latent heat flux from the soil source*	W m^{-2}
LE_{lys}	*Latent heat flux from the understory measured by the lysimeter*	W m^{-2}
LST	*Radiometric Land Surface Temperature*	K
l_w	*Average/effective leaf width*	m
$NDVI$	*Normalized difference vegetation index*	-
R_A	*Aerodynamic resistance to heat transfer*	s m^{-1}
Rn	*Net radiation flux*	W m^{-2}
Rn,c	*Net radiation flux at canopy source*	W m^{-2}
Rn,s	*Net radiation flux at soil source*	W m^{-2}
R_S	*resistance to heat transfer in the boundary layer above soil layer*	s m^{-1}
R_X	*the bulk canopy resistance to heat transfer*	s m^{-1}
T_{AC}	*Air temperature in the canopy space*	K
T_c	*Vegetation canopy temperature*	K
T_s	*Soil surface temperature*	K
w_c	*Canopy width to height ratio*	-
χ_{LAD}	*Campbell 1990 leaf inclination distribution function chi parameter*	-
$z0_{soil}$	*Bare soil aerodynamic roughness length*	m

1. Introduction

Land surface models, mathematical representations of surface-atmospheric exchanges, are important tools to understand fluxes of energy and mass, which drive climatic and Earth system processes (Bonan and Doney, 2018). Heterogeneous vegetated surface layers, where different structural and physiological characteristics must be integrated in both space and time, add important complexities to these models, due to their substantial impact on energy budget partitioning. Horizontal and vertical complexities of vegetated components, along with temporal and phenological dynamics, present notable challenges for Earth observation techniques to model and monitor ecosystem functional properties. Knowledge of these processes are crucial to understand the response of ecosystems to climate and environmental changes, and Earth system dynamics (Krinner et al., 2005; Richardson et al., 2013). Latent heat flux (LE), the aggregated water flux consisting of evaporation from the soil and other wet surfaces (LE_s) and plant transpiration (LE_c), has recently been the subject of extensive research (Stoy et al., 2019). It is a key process that interlinks the water and energy budget along with carbon cycling through the processes of transpiration and photosynthesis (Jasechko et al., 2013). Surface energy balance models, which exploit radiometric land surface temperature (LST) as a key boundary condition, are often used to estimate LE using remote sensing data (e.g. Kalma et al., 2008; Kustas and Anderson, 2009). The two-source energy balance (TSEB) model (Kustas and Norman, 1999; Norman et al., 1995) is such a model that has been widely applied in a variety of landscapes (e.g. Andreu et al., 2018; Gonzalez-Dugo et al., 2009; Guzinski et al., 2013; Kustas et al., 2016; Nieto et al., 2019), which explicitly separates the temperature and energy exchange considering two distinct layers: vegetation and soil.

Surface energy balance models have different degrees of complexities related to the modeling procedure and parameterization. Sensitivity analyses (SA) are instrumental to understand model dynamics and uncertainties by providing insight in how parameters affect model outputs (Song et al., 2015). Model uncertainty stems from three main sources: 1) errors associated with input data, 2) imperfection of model structure, and 3) uncertainty in model´s parameters (Jin et al., 2010; Migliavacca et al., 2012). Different SA methods exist which are often distinguished between local and global techniques (van Griensven et al., 2006). Local methods compute the main response (1^{st} order) or, in other words, the effect a change in a parameter value, while keeping other parameters constant, has on the model output (i.e. one-at-a-time). Global methods evaluate the whole parameter space simultaneously and, thus, compute both the main effect (1^{st} order) and the interactions between parameters (2^{nd} and higher orders) to obtain the total parameter contribution (total order) to variability in model output. Local SA techniques are unsuitable for complex non-linear models since there are often strong and significant parameter interactions (Pianosi et al., 2017; Rosolem et al., 2012). While other studies have investigated the sensitivity of specific parameters or inputs within TSEB (e.g. Alfieri et al., 2019; Andreu et al., 2018; Gan and Gao, 2015; Li et al., 2005) or performed a SA to optimize TSEB (e.g. Diarra et al., 2017), a comprehensive SA for TSEB has not been discussed in the literature, especially for complex ecosystems, such as tree-grass ecosystems (TGE), where surface heterogeneity may potentially lead to increases in parameterization and complexities.

TSEB was originally developed for homogeneous cover types, however, adaptations to the model framework have been implemented to better depict partial canopy cover. These include the addition of vegetation clumping index for radiation interception and transmission (Kustas and Norman, 1999) (section 2.2.1) and a more physically based within-canopy wind attenuation scheme, incorporating the effect of canopy structure, as proposed by Massman et al. (2017) (e.g. Nieto et al., 2019). However, as Andreu et al. (2018) demonstrated, further adaptations to the model structure and parameters may be necessary to simulate fluxes over TGEs due to their complex features. Since TSEB treats the vegetated layer as a single ´big leaf', the parameterization and application of this model poses greater difficulty in a TGE landscape where multiple, different and structurally complex vegetation covers are present. Additionally, in these ecosystems, the degree in which each type of vegetation (i.e. tree and grass) influence land-surface interactions changes throughout the year depending on their differentiated phenological stages (Luo et al., 2018). During the growing season, trees and the grass understory, along with underlying soil, all interact to contribute to the radiative transfer and turbulent exchanges (Baldocchi et al., 2004). However, during the dry summer periods, the grass layer senesces due to meteorological conditions (i.e. water availability, air temperature, vapor pressure deficit), converting the system into (nearly) bare, rather rough, soil with scattered trees, substantially changing land-atmospheric dynamics (Perez-Priego et al., 2018). To account for these spatial and temporal complexities, TSEB was adapted here to consider different modeling periods assuming a dominant vegetation type is present for different seasonal periods. The model simulations were divided considering the two major phenological periods, based on when the grass layer is active during the growing season and not active (i.e. senesced) during the dry summer period.

The main objective of this work is to assess whether this relatively simple adaptation to TSEB, by considering two distinct modeling periods throughout the year and avoiding additional parameters or changes to the basic model structure, was able to reproduce reliable estimations of turbulent energy fluxes for a spatially and temporally complex TGE. To achieve this and to better understand model dynamics, SAs were performed on both model parameters and inputs to quantify and pinpoint the different sources of uncertainties within the modeling procedure. The Sobol' global SA (Saltelli et al., 2010; Sobol′, 2001) method was used on the main parameters within TSEB combined with a local SA of the two main remote sensing based inputs: LST and leaf area index (LAI). The modified model results were evaluated against three independent eddy covariance (EC) systems, including partitioned LE (Perez-Priego et al., 2018), and lysimeter measurements located within the Majadas de Tiétar experimental site (Perez-Priego et al., 2017).

2. Materials and Methods

2.1 Study Site

The TSEB model was applied to estimate energy fluxes in a TGE located in Majadas de Tiétar (39°56′24.68″N,

5°46′28.70″W) in central Spain (Casals et al., 2009; El-Madany et al., 2018). TGE ecosystems are prevalent, covering nearly 15% of the total Earth surface (Friedl et al., 2010), and are notably valuable in both an economic (i.e. livestock grazing) and ecological (i.e. biodiversity and carbon sequestration) sense. Majadas de Tiétar is a well-established experimental site where scattered oak trees, mostly Holm Oak (*Quercus ilex* L.), mix with an herbaceous vegetation understory or grass layer. Holm Oak trees cover roughly 20% of the total land surface at the study site and stand at a mean height of 8 m (El-Madany et al., 2018). The site is a managed semi-natural agroforest (Spanish 'dehesa') with low-intensity grazing from livestock (< 0.3 cows ha^{-1}). It lies within a continental Mediterranean climate region with mean annual temperature of 16.7 ºC and annual precipitation of about 650 mm (with significant inter-annual variability) (Luo et al., 2018). The area is characterized by very hot and dry summer periods (June to September), with grass rapidly drying and senescing during these periods. The average grass LAI ranges roughly between 0.3 – 3.0 m^2m^{-2} throughout the year and can present high variability in spring period (between 0.5 - 2.5 m^2m^{-2}) due to its spatial heterogeneity (El-Madany et al., 2018; Migliavacca et al., 2017). Trees have developed extensive root systems enabling them to survive during long drought periods and, thus, have less temporal variability (mean tree LAI ranging between 1.39 - 1.75 $m^2 m^{-2}$). As such, the distinct survival strategies between grass and tree species allow for coexistence. Three EC towers are present within this experimental site and provided input data for this study. They are located relatively close to each other (< 650 m, Fig. 1) with similar properties within their footprint, but belong to a large scale manipulation experiment, where nitrogen was added to the northern tower (NT), nitrogen and phosphorus were added to the southern tower (NPT) and the central tower kept as a control (CT) (El-Madany et al., 2018.; Luo et al., 2018). This nutrient manipulation experiment was shown to have caused differences in surface biophysical properties and energy partitioning between the three tower footprints (El-Madany et al., 2018; El-Madany et al., in review), making it interesting to evaluate the model runs using these different towers, which have a certain degree of spatial variability in ecosystem functioning.

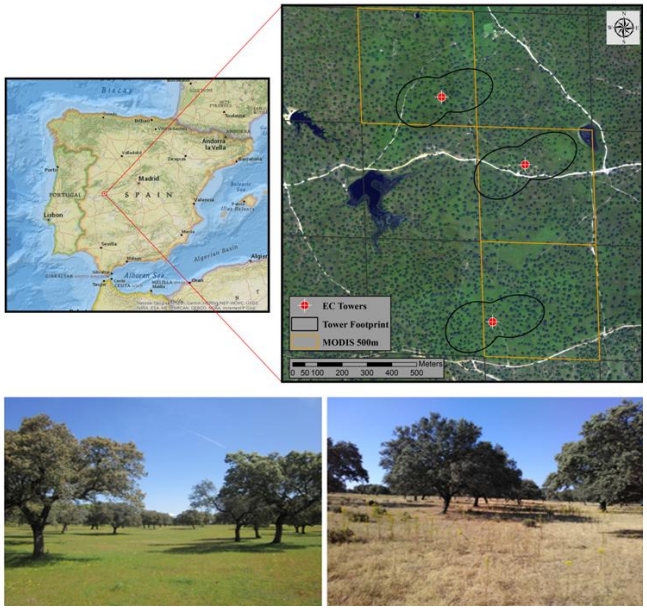

Figure 1. Majadas experimental site and location of the three EC towers indicated by red points, with respective footprints (60% iso-lines for the period of March 2014 until January 2017 and estimated according to Kljun et al.,2015) in early spring (lower left) and summer (lower right). Selected MODIS 500m pixels for LAI estimations (section 2.3.2) are highlighted in orange. The upper left panel reference map was created using ArcMap 10.3 online basemaps (ESRI. 'National Geographic', http://www.arcgis.com/home/item.html?id=30e5fe3149c34df1ba922e6f5bbf808f, 13 December 2011)

2.2 TSEB Model Overview

The TSEB model was first proposed in Norman et al. (1995), with important adjustments described in Kustas and Norman (1999). Its main inputs are LST, derived from thermal infrared (TIR) radiation, vegetation structural properties (e.g LAI, canopy height) and meteorological forcing (irradiance, air temperature and wind speed). The principle source of uncertainty within TSEB lies in the estimation of the sensible heat flux (H), which is calculated through the heat transport equation (eq. 1).

$$H = \frac{\rho C_p (T_o - T_A)}{R_H} \quad (1)$$

where H is sensible heat flux (W m^{-2}); ρC_p is the volumetric heat capacity of air (J m^{-3} K^{-1}); T_o is the aerodynamic temperature of the surface (K); T_A is the air temperature at a reference/measurement height (K); and R_H is the aerodynamic resistance to heat transport (s m^{-1}). The heat transport equation is satisfied when using aerodynamic surface temperature (i.e. surface temperature at the canopy source-sink height), however, LST obtained from TIR remote sensing (i.e. skin radiometric surface temperature) can differ up to several degrees compared to the aerodynamic surface temperature (Norman et al., 1995), and their relationship is not well established (i.e. Colaizzi et al., 2004). TSEB, thus, tackles this by assuming that the total blackbody thermal radiance that is emitted by the bulk surface is weighted by the fraction of vegetation

observed by the sensor and the emission of both soil and vegetation surfaces, as expressed in eq. 2 taken from Norman et al. (1995):

$$LST(\theta) = \left[f(\theta)T_c^4 + \left(1 - f(\theta)\right)T_s^4\right]^{1/4} \quad (2)$$

where $f(\theta)$ is the fraction of vegetation observed by the TIR sensor at an angle θ and is mainly a function of LAI; T_c is the vegetation canopy temperature (K); and T_s is the soil surface temperature (K). Using this scheme, TSEB avoids the use of an empirical method to link radiometric and aerodynamic surface temperature, such as the use of excess resistance in SEBS (Su, 2002) or the use of hot and cold end member pixels as in METRIC (Allen et al., 2007) or SEBAL (Bastiaanssen et al., 1998). Using this two-layer approach, the energy balance is formulated in TSEB for each of the layers separately as follows:

$$\begin{aligned} R_{N,c} &= LE_c + H_c \\ R_{N,s} &= LE_s + H_s + G \end{aligned} \quad (3)$$

where R_N is the net radiation (W m^{-2}); LE is latent heat flux (W m^{-2}); G is the soil heat flux (W m^{-2}); and subscript s and c refer to soil and vegetation canopy layers, respectively. Note that horizontal heat advection, canopy heat storage as well as the energy used for CO_2 fixation are neglected in eq.3. Radiative transfer and absorption through the canopy ($R_{N,c}$ and $R_{N,s}$) are simulated through an exponential radiation extinction function as described in chapter 15 of Campbell and Norman (1998), considering spectral differences in shortwave and longwave radiation and direct and diffuse radiation as incorporated in Kustas and Norman (1999). H is derived using an in 'series' resistance network (Norman et al., 1995) (Fig. 2), and applying eq. 4 to 6, which allows for heat turbulent interchange between the canopy and soil layers:

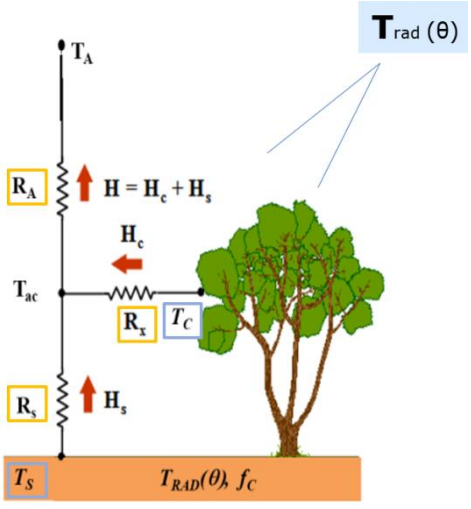

Figure 2. TSEB Sensible Heat model scheme (adapted from Kustas and Anderson, 2009)

$$H_s = \frac{\rho C_p (T_s - T_{ac})}{R_S} \quad (4)$$

$$H_c = \frac{\rho C_p (T_c - T_{ac})}{R_X} \quad (5)$$

$$H = H_s + H_c = \frac{\rho C_p (T_{ac} - T_A)}{R_A} \quad (6)$$

where T_{ac} is the air temperature in the canopy space (K) and is equivalent to the aerodynamic temperature (T_0); R_S is the resistance to heat transfer in the boundary layer above soil layer (s m^{-1}); R_X is the bulk canopy resistance to heat transfer (s m^{-1}); R_A is the aerodynamic resistance to heat transfer based on the Monin-Obukhov similarity theory. Refer to appendix A of Norman et al. (1995) for details on the series resistance scheme.

Since eq. 2 has two unknowns (T_c and T_s), the canopy layer is assumed, as a first estimate, to be initially transpiring at a potential rate (LE_{ci}) using, in this case, the Priestley-Taylor formulation:

$$LE_{ci} = \alpha_{PT} f_g \left(\frac{\Delta}{\Delta + \gamma}\right) R_{N,c} \quad (7)$$

where LE_{ci} is the initial canopy transpiration estimate (W m^{-2}); α_{PT} is the Priestley-Taylor coefficient (default is 1.26), defined in this case only for the canopy component (Kustas and Anderson, 2009) (-); f_g is the fraction of vegetation that is green and hence actively transpiring (-); Δ is the slope of the saturation vapor pressure curve at air temperature T_A (kPa K^{-1}); and γ is the psychrometric constant (kPa K^{-1}). This initial assumption, where the canopy is transpiring without water stress, allows to solve all the systems of equations presented above (eq. 2 to 7). However, if the vegetation is stressed, the Priestley-Taylor formulation will overestimate the transpiration of the canopy, which, in order to conserve the total surface temperature and energy balance in eqs. 2 and 3, will result in unrealistic soil condensation (i.e. negative fluxes). As it is assumed that condensation does not occur during daytime convective conditions, an iteration procedure is applied that reduces α_{PT} until realistic soil fluxes area achieved (i.e. $LE_s \geq 0$). A more complete discussion on conditions that reduces α_{PT} is given in Anderson et al. (2005) and Li et al. (2005). For more implementation details, the reader is referred to the source code (*https://github.com/hectornieto/pyTSEB*) and Norman et al. (1995).

2.2.1 Radiation transmission in sparse vegetation

The structure and distribution of foliage in the vegetative layer has a significant impact on the dynamics of radiation interception and transmission through the canopy (Anderson et al., 2005; García et al., 2015; Kustas and Norman, 1999).

This in turn has a very important implication for radiometric temperature partitioning between the soil and vegetation components and their resulting contribution to heat fluxes (Anderson et al., 2005). The original TSEB radiative transfer equations assume a randomly distributed homogenous (non-clumped) canopy (Norman et al., 1995). However, sparse vegetation is generally clumped and tends to intercept less radiation for the same LAI compared to vegetation randomly dispersed over the surface (Campbell and Norman, 1998; Kustas and Norman, 1999). As such, the clumping index (Ω) quantifies the spatial distribution of foliage to account for non-randomness in vegetated structures. LAI is multiplied by the clumping factor to obtain effective LAI (ΩLAI). As incorporated in Kustas and Norman (1999), TSEB estimates Ω as a function of the difference between the canopy gap fraction compared to a homogenous case using eq. 8 (section 2 in Kustas and Norman, 1999) and estimating the beam extinction coefficient assuming an ellipsoidal leaf angle distribution (LAD) with eq. 9 (section 15.2 in Campbell and Norman, 1998).

$$\Omega(0) = \frac{-\ln(f_c \exp(-k_{be}F) + (1 - f_c))}{k_{be}\mathrm{F}} \tag{8}$$

$$k_{be} = \frac{\sqrt{{\chi_{LAD}}^2 + \tan^2(0)}}{\chi_{LAD} + 1.774(\chi_{LAD} + 1.182)^{-0.733}} \tag{9}$$

Where $\boldsymbol{\Omega}(0)$ is the clumping index when the vegetation canopy is viewed at nadir (-); k_{be} is the beam extinction coefficient (-) based on a ellipsoidal LAD (Campbell and Norman, 1998); f_c is the vegetation fractional cover (-); F is the local LAI (LAI/f_c); and χ_{LAD} is the leaf inclination distribution function chi parameter (-) (Campbell and Norman, 1998). Ω is also dependent on the solar zenith angle (θ_s) and is estimated using eq. 10 as described in section 15.13 of Campbell and Norman (1998).

$$\Omega(\theta_S) = \frac{\Omega(0)}{\Omega(0) + [1 - \Omega(0)]\exp[-2.2(\theta_S)^{\mathrm{p}}]} \tag{10}$$

where $p = 3.8 - 0.46(\frac{1}{w_c})$; and w_c is the vegetation´s width to height ratio (-).

2.2.2 Resistances within and below canopy

The semi-empirical derivations of R_S and R_X, as introduced in Norman et al. (1995) and Kustas and Norman (1999), are dependent on wind speeds below and within the vegetative canopy, respectively (eq. 11-12).

$$R_S = \frac{1}{c(T_s - T_c)^{1/3} + bu_s} \tag{11}$$

$$R_X = \frac{C'\sqrt{l_w/u_{d_o+z_{0m}}}}{LAI} \quad (12)$$

where u_s is the wind speed just above the surface where the impact of soil roughness is minimal (i.e. . $z_{0,soil}$) (ms^{-1}); $u_{d_o+z_{om}}$ is the wind speed within the canopy-air interspace at the height of momentum source/sink (ms^{-1}); l_w is the effective leaf width size (m); and c ($m\ s^{-1}\ K^{-1/3}$), b (-) and C' ($s^{1/2}\ m^{-1}$) are coefficients taken from Kustas and Norman (1999) and Norman et al. (1995), based on the works of Sauer and Norman (1995), Kondo and Ishida (1997) and McNaughton and Van Den Hurk (1995) (default values are 0.0025 $m\ s^{-1}\ K^{-1/3}$, 0.012 and 90 $s^{1/2}\ m^{-1}$ respectively). u_s and $u_{d_o+z_{0m}}$ in eq. 11 and 12 are both derived from an observed wind speed above the canopy that is extrapolated through and below the canopy based on the exponential wind attenuation law (Goudriaan, 1977). TSEB determines the two key roughness parameters, the zero-plane displacement height (d_0) and the aerodynamic roughness length for momentum transfer (z_{0m}), from the vegetation structure. When considering the grass canopy layer, the traditional fixed ratio to canopy height method is used to estimate d_0 and z_{0m} (Campbell and Norman, 1998*)*. In the case of the tree canopy layer, a different approach is used, which additionally considers the canopy shape and density´s effect on the roughness parameters. This study follows the procedure described in Schaudt and Dickinson (2000), which stems from the work of Raupach (1994) and Lindroth (1993*)*, and is generally viewed as more suitable for tall wooded vegetation. These methods do not apply corrections associated to the roughness sub-layer (e.g. Weligepolage et al., 2012*)*. However, Alfieri et al (2019) found that the TSEB modeled fluxes were largely insensitive to differences in estimated d_0 and z_{0m} obtained from various methods.

2.3 Data

2.3.1 Eddy covariance and bio-meteorological measurements

The three EC towers (CT - FLUXNET identifier ES-LMa, NT – FLUXNET ID ES-LM1, and NPT – FLUXNET ID ES-LM2), simultaneously operating within the Majadas study site, provided all necessary inputs to run TSEB (table 1), except for continuous vegetation LAI estimates (section 2.3.2). H and LE estimations from the EC system served to benchmark model performance. Details on the data processing are found in El-Madany et al. (2018). Data were obtained between the period of 2015-01-01 and 2017-12-31. Since TSEB closes the energy balance by definition, energy balance closure of the EC flux measurements was ensured by allocating the residuals to the observed LE, assuming that errors in LE are larger than H due to issues related to the instrumentation (Foken et al., 2011), as in previous studies (e.g. Guzinski et al. 2014; Kustas et al. 2012). Measurements from 2015 of the CT tower were selected as the 'main' simulation site/period. It was used to perform the SA (section 2.4.3) and to adapt the model for seasonality (section 2.4.4). Other towers (NT and NPT) and years (2016 and 2017) provided independent evaluations of model performance (section 2.4.5).

While TSEB has used different methods to estimate ground heat flux (G) (Norman et al., 1995; Santanello and Friedl, 2003), this study directly forced in situ G measurements as a model input to limit uncertainty and noise in turbulent flux estimations

associated with errors in G. The weighted average of 8 soil heat flux plates represented G at the ecosystem level. They were located both in open grass and below tree canopy and weighted to consider shadow effects throughout the day. Note that corrections related to heat storage above the soil heat flux plates were not applied and, as such, G is likely slightly underestimated. The radiometric LST was estimated using longwave radiation measurements from the 4-component radiometer CNR4 (Kipp & Zonen, Delft, Netherlands) (eq.13), which has roughly between 19-25% of tree cover within its field of view for the three towers (i.e. CT, NT and NPT) used. This is roughly the same average tree contribution to the EC footprint as reported in El-Madany et al. (2018).

$$LST = \left(\frac{L_{out} - (1 - \varepsilon_{surf})L_{in}}{\sigma \varepsilon_{surf}}\right)^{1/4}$$

$$\varepsilon_{surf} = f_c 0.99 + (1 - f_c)0.94 \quad (13)$$

where L_{out} and L_{in} are upwelling and downwelling longwave radiance; σ is the Stephan-Boltzman constant; ε_{surf} is the surface emissivity; and f_c is the vegetation fractional cover. The values of 0.99 and 0.94 in eq. 13 correspond to the broadband emissivity for vegetation and bare soil respectively (Sobrino et al., 2005).

275 **Table 1**. Data used to parameterize and evaluate the TSEB model

Parameter/Variable	Description	Source	Purpose
LST	Land surface temperature (K) estimated from longwave radiation using eq.13	4-component radiometer (CNR4, Kipp & Zonen, Delft, Netherlands)	Model input
LAI	Leaf area index (m^2/m^2) based on NDVI (appendix A)	MODIS/Terra and Aqua Nadir BRDF-adjusted Reflectance Daily L3 500m v006 (MCD43A4) product	Model input
T_a	Air temperature (K) measured at 15m	Hygro.Thermo transmitter	Input forcing
RH	Relative humidity (%) measured at 15m	Hygro.Thermo transmitter	Input forcing
u	Wind speed (m/s) measured at 15m	Sonic anemometer (Gill R3-50, Lymington UK)	Input forcing
P	Atmospheric pressure (mb)	Barometric pressure sensor	Input forcing
S_{dn}	Incoming shortwave irradiance (W m^{-2})	4-component radiometer (CNR4, Kipp & Zonen, Delft, Netherlands)	Input forcing
G	Soil heat flux (W m^{-2})	Soil heat flux plates	Input forcing
L_{in}	Incoming longwave irradiance (W m^{-2})	4-component radiometer (CNR4, Kipp & Zonen, Delft, Netherlands)	Estimate LST and input forcing
L_{out}	Outgoing longwave irradiance (W m^{-2})	4-component radiometer (CNR4, Kipp & Zonen, Delft, Netherlands)	Estimate LST
α_{PT}	Priestley Taylor coefficient for canopy potential transpiration (-)	Default value (Norman et al., 1995; Kustas and Norman, 1999)	Model parameter
f_g	Fraction of vegetation that is green (-)	Study site information (El-Madany et al., 2018)	Model parameter
f_c	Fractional cover (-)	Study site information (El-Madany et al., 2018)	Model parameter
w_c	Canopy width to height ratio (-)	Default value (Campbell and Norman, 1998)	Model parameter
X_{LAD}	Campbell 1990 leaf inclination distribution function chi parameter (-)	Default value (Campbell and Norman, 1998)	Model parameter
h_c	Canopy height (m)	Study site information (El-Madany et al., 2018)	Model parameter
$z0_{soil}$	Bare soil aerodynamic roughness length (m)	Default value (Norman et al., 1995)	Model parameter
l_w	Average/effective leaf width (m)	Default value (Norman et al., 1995)	Model parameter
b	Soil-surface resistance (Rs) constant (-)	Default value (Kustas and Norman, 1999; Sauer and Norman, 1995)	Model parameter
c	Soil-surface resistance (Rs) constant (m s-1 K-1/3)	Default value (Kondo and Ishida, 1997; Kustas and Norman, 1999)	Model parameter
C’	Constant in total boundary resistance (Rx) ($s^{1/2}$ m^{-1})	Default value (McNaughton and Van Den Hurk, 1995; Kustas and Norman, 1999)	Model parameter
H	Sensible heat flux (W m-2)	3D sonic anemometer (Gill R3-50 , Lymington UK)	Model evaluation
LE	Latent heat flux (W m^{-2})	IRGA (Li-7200, Licor, Lincoln Nebraska, USA) and 3D sonic anemometer (Gill R3-50, Lymington UK)	Model evaluation
LE_{lys}	Latent heat flux from the understory measured by lysimeters (W m-2)	Weighing-lysimeters (Perez-Priego et al., 2017)	Model evaluation
$LE_{c,PP}$	Canopy transpiration flux estimated (W m-2) as in Perez-Priego et al. 2018	Perez-Priego et al., 2018	Model evaluation

2.3.2 Vegetation biophysical measurements

In situ grass LAI measurements were acquired in the context of the FLUXPEC project (http://www.lineas.cchs.csic.es/fluxpec/) at eleven plots (25mx25m) randomly placed around the CT in nineteen field campaigns between 2013-10-31 and 2016-11-16 (Mendiguren et al., 2015). Destructive samples were collected in two 25cmx25cm quadrants within each plot and LAI was derived using gravitational methods, where green and non-green elements were separated to compute both total and green LAI (and hence f_g). Time series of reflectance factors from the MODIS/Terra and Aqua Nadir BRDF-adjusted Reflectance Daily L3 500m v006 (MCD43A4) product were acquired for pixels centered in each of the three towers (Fig. 1). The 500m by 500m pixel size was deemed adequate to characterize the tower footprint (Pacheco-Labrador et al., 2017). The normalized difference vegetation index (NDVI) was derived using band 1 (red: 620nm-670nm) and band 2 (NIR: 841nm-876nm) as follows:

$$NDVI = \frac{Band2(NIR) - Band1(RED)}{Band2(NIR) + Band1(RED)} \quad (14)$$

An empirical relationship between NDVI and *in-situ* destructive grass LAI measurements was developed specifically for the Majadas experimental site (Appendix A, Fig.A1). In order to obtain the ecosystem LAI adjusted for the tree canopy effect within the tower footprint, *in-situ* tree LAI measurements were incorporated to achieve a weighted average between tree (20%) and grass (80%). The average tree LAI acquired using the LAI-2200 plant canopy analyzer (LAI-2200) (LICOR Bioscience USA, 2011) during five field campaigns at different seasonal periods between 2017-2018 was used as a reference year. Local tree LAI ranges between 1.39 and 1.75 $m^2\ m^{-2}$ (about 0.3 $m^2\ m^{-2}$ effective/landscape LAI) and has low inter-annual variability (Luo et al., 2018). Linear interpolation between sampling dates was performed to obtain a continuous daily time series. Refer to figure 3 for the ecosystem LAI time series for the different towers and years and to figure 4 for grass, tree and ecosystem LAI time series used for the main modeling site/period (i.e. 2015 at CT tower).

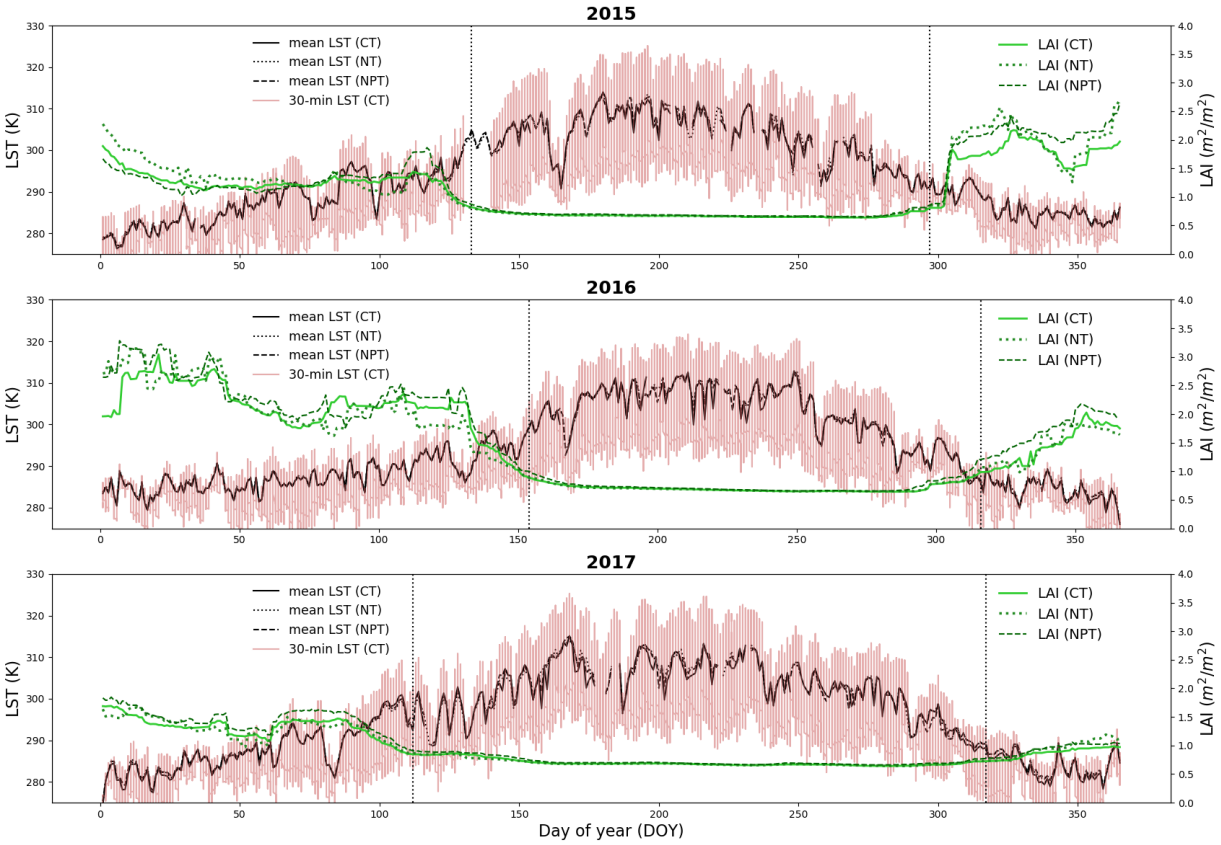

Figure 3 Annual time series of half-hourly LST (red), daily mean LST (black) and ecosystem LAI for CT (green), NT (purple) and NPT (blue) for years 2015, 2016 and 2017. Vertical dashed lines indicate transition dates used for TSEB-2S (section 2.4.4)

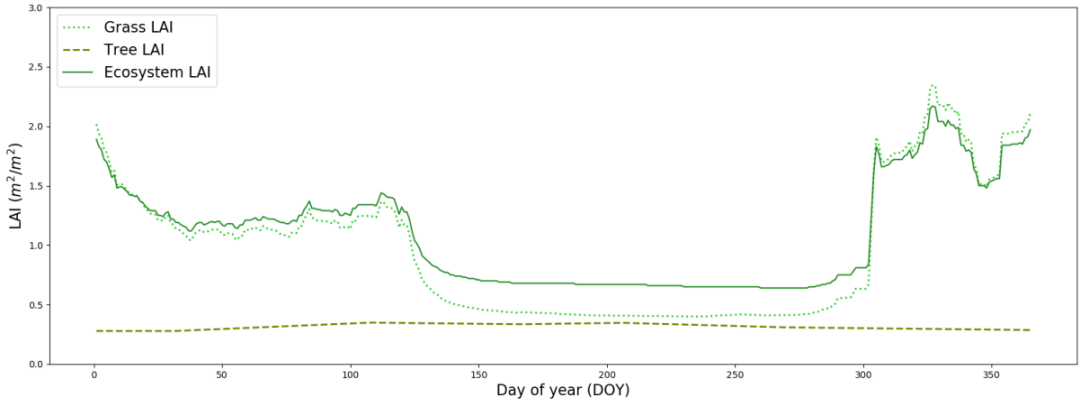

300

Figure 4. Grass, tree and ecosystem LAI time series for at the CT tower for 2015. Note that tree LAI shown here refers to the effective (landscape) LAI meaning that the tree based measurement was weighted by its fractional cover (i.e. 0.2)

2.4 Model Simulations and Evaluation

Prior to conducting the simulations with TSEB, global and local SAs were performed on the main parameters and inputs, respectively. Both SAs were conducted using the default TSEB model (section 2.4.1). In addition, two end member simulations, where either a pure grassland or broadleaf forest was assumed for the entire year, were performed to better understand the effect of the vegetation canopy on simulated fluxes for extreme cases (section 2.4.3). The model was then adapted considering two distinct seasonal periods, each having a dominating vegetation layer (section 2.4.4). Parameters found to have large influence through the SA (section 2.4.2) were adapted for each period in order to characterize the assumed prominent vegetation (i.e. either as tree or grass). All simulations were evaluated for daytime fluxes (i.e. when S_{dn} > 50 Wm^{-2}) since TSEB is designed to model fluxes for daytime conditions with remote sensing data.

2.4.1 Default TSEB model configuration

In this default configuration (hereafter as TSEB-DF), the vegetated layer was parameterized attempting to depict the mix between tree and grass observed over tower footprint, where the vegetation cover was dominated by grass but the turbulent resistances were assumed to be largely affected by the sparse tree layer (El-Madany et al., 2018). As such, ecosystem LAI (weighted average of grass and tree LAI, Fig. 3 and 4) was used as input and vegetation resistances and roughness were derived using the weighted average of grass and tree canopy height (h_c = 0.8*0.5 m+0.2*8 m= 2m). The roughness parameters were estimated following the procedure as described in Schaudt and Dickinson (2000). Table 2 summarizes the parameter values used for this default model configuration. The green fraction (f_g) was set to 0.7 being roughly the average value observed from grass field measurements. The model simulations were performed at the sub-hourly (30-mins) time step for 2015 over the CT EC footprint and benchmarked against EC derived LE and H.

Table 2. Parameter values of the TSEB-DF model configuration

Parameters	TSEB-DF	Source
α_{PT} (-)	1.26	Norman et al., 1995; Kustas and Norman, 1999
f_g (-)	0.7	Study site information (El-Madany et al., 2018)
f_c (-)	1	Study site information (El-Madany et al., 2018)
w_c (-)	1	Campbell and Norman, 1998
X_{LAD} (-)	1	Campbell and Norman, 1998
h_c (m)	2	Study site information (El-Madany et al., 2018)
$z0_{soil}$ (m)	0.01	Norman et al., 1995
l_w (m)	0.01	Norman et al., 1995
b (-)	0.012	Kustas and Norman, 1999; Sauer and Norman, 1995
c ($m\ s^{-1}\ K^{-1/3}$)	0.0025	Kondo and Ishida, 1997; Kustas and Norman, 1999
C' ($s^{1/2}\ m^{-1}$)	90	McNaughton and Van Den Hurk, 1995; Kustas and Norman, 1999

2.4.2 Sensitivity Analysis

Sobol´ Global Parameter Sensitivity Analysis

Variance-based SA methods are now more prominently used (Rosolem et al., 2012*)*. They decompose the total variance between simulated and observed data into various parts determining the contribution of the different parameters and their combined interactions on total output variance. Multiple model simulations are required with different parameter sets to quantify the model output variance in regard to the variation in the parameter space.

The Sobol' SA method was used as it is able to compute the 1st, 2nd and total order sensitivity indices. The main disadvantage of the Sobol' method is the high computational cost, where many simulations are required to obtain robust results within a sufficient confidence level. To apply this methodology, a selection of model parameters and their respective bounds were configured. Based on this, parameters sets for n simulations were generated using the Sobol sequence (Saltelli et al., 2010; Sobol′, 2001), a quasi-random method with quasi-Monte-Carlo integration, which typically samples bounded space more uniformly than completely random sequences (Zhang et al., 2015).

$$y = f(\theta) = f(\theta_1, \theta_2, \theta_3 \dots, \theta_n) \tag{15}$$

where y is an indicator of the model performance and $\{\theta_1, \theta_2, \theta_3 \dots, \theta_n\}$ is the model parameter set which controls the model behavior and, thus, its performance, y. The Sobol' approach decomposes the variance observed in y through the variance in all θ factors by separating parameters into terms of increasing dimensionality, with each successive dimension representing greater interaction of parameters, represented as:

$$Var(y) = \sum_i V_i + \sum_i \sum_{i<j} V_{ij} + \cdots + V_{1,2\dots,n} \tag{16}$$

where $Var(y)$ is the total output variance; V_i is the portion of variance contributed by parameter θ_1 (also known as the first order variance or main effect); and V_{ij} is the portion of variance attributed through the interaction between θ_i and θ_j and so on. The formula of eq.16 holds if all the parameter factors are independent (Saltelli et al., 2010), which is the case for this study. Parameter values do not correlate and are independently assigned over a uniform distribution between the specified bounds (table 3).

The first-order sensitivity (S_i), second-order sensitivity (S_{ij}) and total order sensitivity (S_{Ti}) indices are calculated using equations 17 to 19 as:

$$S_i = \frac{V_i}{Var(y)} \tag{17}$$

$$S_{ij} = \frac{V_{ij}}{Var(y)} \tag{18}$$

$$S_{Ti} = 1 - \frac{\mathrm{V_{\sim i}}}{\mathrm{Var(y)}} \tag{19}$$

where $V_{\sim i}$ is the average variance depicted when all parameters except for θ_i vary (i.e. θ_i is kept fixed); S_{Ti} represents the contribution of both the direct (1st order) and indirect (sum of 2nd order) effects of θ_i on the total variance, $Var(y)$.

Model variance was calculated based on H since LE is computed through the residual of the energy balance in TSEB, where errors in H are transposed into LE. Root-Mean-Square Deviation (RMSD) was used as the objective function to quantify model output variance for the entire simulation year, where tower-based EC H provided the observed time series.

$$RMSD = \sqrt{\frac{\sum(H_{TSEB<30min>} - H_{EC<30min>})^2}{N}} \tag{20}$$

where $H_{TSEB<30min>}$ is modeled H at a 30 minutes time step; $H_{EC<30min>}$ is the observed EC H; and N is the total number of observations used. The SA was undertaken with TSEB-DF, considering the 11 parameters within TSEB, which are used in the sub-modules of radiation transfer between vegetation and soil, roughness and resistance scheme, and the initial canopy transpiration estimate from the Priestly-Taylor formulation; and their respective bounds were based on literature or the physical limits of the parameter in question (table 3). A total of 45,500 simulations were used for this SA. The Python package SALib (Sensitivity Analysis Library in Python) (Herman and Usher, 2017) was integrated with the Python implementation of TSEB (pyTSEB, https://github.com/hectornieto/pyTSEB) to perform these analyses.

Table 3. Parameters bounds for the Sobol' global SA

Parameter	Lower bound	Upper bound	Sub module within TSEB	Reference
α_{PT}	1.26	2	Initial canopy transpiration estimate	Kustas and Norman, 1999
f_g	0.01	1	Initial canopy transpiration estimate	
f_c	0.1	1	Radiation transfer through canopy	
w_c	0.5	3	Radiation transfer through canopy	
χ_{LAD}	0.5	3	Radiation transfer through canopy	Campbell and Norman, 1998
h_c	0.1	20	Aerodynamic resistances (Ra, Rs, Rx)	
$z0_{soil}$	0.005	0.2	Aerodynamic resistances (Rs)	Norman et al., 1995
l_w	0.005	0.1	Aerodynamic resistances (Rs, Rx)	
b	0.012	0.087	Aerodynamic resistances (Rs)	Sauer and Norman, 1995
c	0.0011	0.0038	Aerodynamic resistances (Rs)	Kondo and Ishida, 1997
C‘	50	150	Aerodynamic resistances (Rx)	McNaughton and Van Den Hurk, 1995

Input Local Sensitivity Analysis

Errors associated to the remote sensing derived input data (i.e. LST and LAI) are another important source to the total output uncertainty. Since input data is fluctuating at every time step, a different method was needed compared to the method used for the static parameters described above. Random white noise, mimicking potential errors, over a uniform distribution of +- 3K and +- 0.4 m^2 m^{-2} were added to the 'observed' LST and LAI, respectively. The range of errors in LST was chosen to fit within the typical uncertainties associated with remote sensing based LST retrievals over vegetation (e.g. Sobrino et al., 2006). The range in LAI perturbation was based on the errors associated with the LAI empirical model used in this study (appendix A). The Sensitivity indices (SI) were then computed based on the partial derivative of the output result with respect to change in input caused by the implemented random noise, using eq. 21 adapted from van Griensven et al. (2006).

$$SI = \frac{\frac{M(\Delta\rho_i + \rho_j + \cdots + \rho_k) - M(\rho_i + \rho_j + \cdots + \rho_k)}{M(\rho_i + \rho_j + \cdots + \rho_k)}}{\frac{\Delta\rho_i}{\rho_i}} \quad (21)$$

where M is model output; ρ refers to the different model inputs; $\Delta\rho_i$ refers to the pertubation of the input caused by artificial noise. The SI is based on the change observed for modeled H.

The input SA was implemented for 365 days (during 2015) with a 30-min time step. Since TSEB incorporates LAI at the daily time scale, the SI is derived based on the daily aggregated absolute change in H in relation to the absolute change in

LAI for that day. For the LST analysis, the effect of a deviation in LST on the resulting H will likely be impacted by the hour in which the deviation occurs (i.e. a perturbation in LST during morning time will likely impact H differently compared to a midday perturbation). To normalize the time of perturbation, for each simulation day, only the mean net perturbation of LST during midday (between 11:00 and 13:00 UTC) was used to analyze the net effect on H during that same time period. Hence, SIs for both LAI and LST were derived for each daily time step using the absolute change in inputs with the resulting absolute change in output (i.e. H).

2.4.3 End Member Simulations

In addition to the TSEB-DF simulations, two 'end member' scenarios were conducted as limiting case studies. The first case assumes a pure grassland, ignoring the tree components, for the entire year (hereafter as $TSEB_{grass}$). The second case ignores the grass layer, simulating the vegetated component as a scattered evergreen broadleaf forest (hereafter as $TSEB_{tree}$). The estimation of the roughness characteristics differed for each scenario as described in section 2.2.2 (i.e. fixed ratio for grass layer and the method of Schaudt and Dickinson (2000) when considering tree canopy) and the most influential parameters (as derived from the SA) were changed to characterize the assumed dominant vegetation. In addition, instead of ecosystem LAI, each end member scenario uses the LAI corresponding to the assumed vegetation layer (i.e. grass or tree LAI as shown in Fig. 4). These scenarios were performed on the CT tower during 2015. These type of 'end member' configurations are typical for models applied at the global scale, which often assign model parameter values based on specific or assumed land/vegetation type, where errors in land classifications, which are common for TGEs, causes for a less accurate parameterization/depiction of surface conditions (e.g. Jung et al., 2006)

2.4.4 Two-Season modeling approach

We propose here an adaptation of the TSEB-DF by using a two-season modeling approach (hereafter as TSEB-2S) that divides the annual simulation into two main phenological periods: a grass dominated growing period (i.e. grass-soil system) and a tree dominated summer/dry period (i.e. tree-soil system). This modeling scheme attempts to depict the considerable changes observed within the different seasonal periods due to phenology. Phenological processes are highly dynamic in this ecosystem (Luo et al., 2018) and these changes in vegetation cover alter the turbulent conditions (i.e. roughness), radiation transmission and, hence, the surface energy balance (Baldocchi et al., 2004). During the summer period, the understory transforms into a dry and rough layer with minimal transpiration from vegetation. Therefore, the TSEB-2S separates the simulation period for these two major conditions observed: 1) the grass is active and transpiring (growing season) and 2) the grass species are senesced and not transpiring (summer). The seasonal transition dates were estimated using an asymmetric gaussian filter over the MODIS-NDVI time series, where the dry period was assumed to begin when vegetation (i.e. NDVI) begins to decay (downward inflection point) and the dry period ends when vegetation (i.e. NDVI) begins to re-green (upward inflection point). For instance, for the simulation year of 2015, the dry period begins on May 13th and ends on October 24th (refer to Fig. 3 for all transitions dates used).

In TSEB-2S, the dry period was parameterized as a tree-soil system, assuming the grass has senesced and the understory is a rough soil. As such, the model was parameterized as the $TSEB_{tree}$ configuration and using tree LAI as input (Fig. 4). By contrast, the growing period was parameterized ignoring the tree canopy and assuming a grass-soil system using the $TSEB_{grass}$ parameterization for this period and grass LAI (Fig. 4). This assumption was supported by the evidence that the understory layer dominates LE in this site (Perez-Priego et al., 2018, 2017).

2.4.5 Model evaluation

TSEB-2S was evaluated using independent model simulations for different spatial (three tower sites) and temporal (three different years) characteristics. To validate and benchmark model performance, the seasonally adapted TSEB-2S was independently tested on three EC towers within the study site (CT, NT and NPT). The towers are located relatively close to each other but have gone through a nutrient manipulation experiment, which was shown to cause differences in surface biophysical properties and energy partitioning between the three tower footprints (El-Madany et al., 2018; El-Madany et al., in review). The model was also benchmarked for different years (2015, 2016 and 2017) with different intra-annual dynamics (Fig. 3). Model performance was evaluated against the observed EC tower measurements in question and quantified with RMSD (eq. 20), mean bias (eq.22) and the Pearson´s correlation coefficient (r).

$$bias = \frac{\sum(H_{TSEB<30min>} - H_{EC<30min>})}{N} \quad (22)$$

Additionally, an evaluation of the modelled LE partitioning, between LE_c and LE_s, was performed. Since TSEB-2S makes the assumption of a different and unique vegetation structure and cover for different seasonal periods, it was interesting to evaluate if the model can also obtain reliable estimates of the LE partitioning along with the bulk fluxes. Modelled LE_s was evaluated against independent lysimeter LE measurements (LE_{lys}) of the understory during the dry summer periods at CT, when the grass is senesced and, thus, LE_{lys} is assumed to be equivalent to soil evaporation (i.e. LE_s). For a detailed description of the lysimeter set-up in the Majadas experimental site, refer to Perez-Priego et al. (2017). In addition, the TSEB-2S simulated LE_c was benchmarked against that derived from a physiologically-based water flux partitioning approach, which allows for the separation of LE measured by EC into transpiration and evaporation components. The method was developed and validated in the same study site (Perez-Priego et al., 2018).

3. Results

3.1 TSEB-DF sensitivity analysis

3.1.1 Sobol´ parameter SA

The parameter global SA showed that f_c had the largest impact on model results, both as the main effect (S_i) and through its interactions with other parameters (S_T) (Fig. 5). In general, parameters related to vegetated structure (h_c) and cover (f_c and f_g) demonstrated the largest sensitivity. Notably, many parameters had low first order sensitivities (close to 0) but relatively important total order sensitivities, indicative of large interactions between parameters. The *b* parameter, used in the computation of $R_{S,}$ was the only more empirically derived parameter that demonstrated a relatively high influence on modelled output.

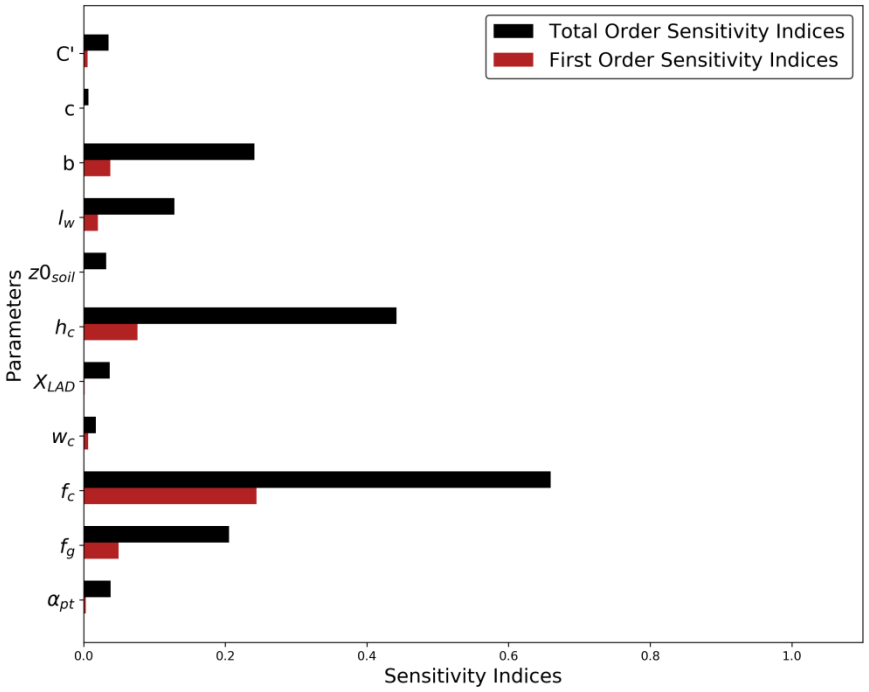

Figure 5. First (S_i) and total (S_T) order SI for the main parameters in TSEB-DF

3.1.2 Input local SA

Uncertainties related to LST and LAI showed important impacts on model results (Fig. 6). Simulated H is particularly sensitive to deviations in LST, where differences of a unit change of LST (Δ 1K) is associated to a median 17.3% change in

modelled H. The uncertainty in LAI demonstrated, compared to LST, relatively less influence on H. A 0.1 m^2/m^2 change in LAI is associated with a 2.9% change in simulated H with TSEB-DF.

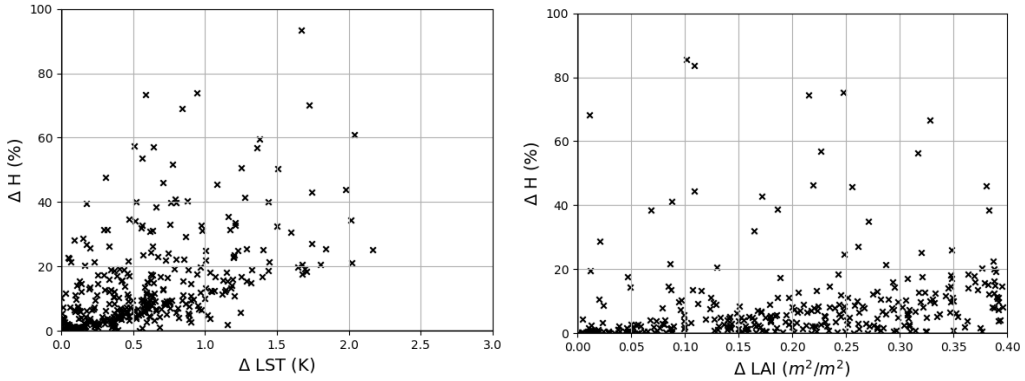

Figure 6.Scatter plots of the absolute percent change in daily aggregated H (y-axis) with the associated absolute perturbation of the daily aggregated input (x-axis): LST (left) and LAI (right) using TSEB-DF

3.2 $TSEB_{grass}$, $TSEB_{tree}$ and TSEB-2S model configuration

The global SA results illustrated in Fig. 5 showed that parameters related to the vegetation cover (i.e. f_c and f_g) and structure (i.e h_c) had the most influence on model performance. Since these are physical and measureable parameters, these were set for each end-member scenario (section 2.4.3) according to the assumed dominant vegetation as described in table 4. The f_g was set to 0.7 for the grass configuration according average field observations, while it was set to 0.9 for the evergreen tree cover to account for the presence of non-photosynthetic material such as branches. The h_c for the tree layer was set to 8m according to the mean height of trees within the study site (El-Madany et al., 2018) and the f_c was set 0.2, this being about the average tree canopy fraction observed for the tower footprints (El-Madany et al., 2018). Additionally, the l_w was increased to 0.05m for the tree cover to better represent the larger leaves of the oak species within the study site. The resistance *b* coefficient, used in the formulation of R_s, was increased for the scattered tree cover, as was successfully tested and implemented in Kustas et al. (2016) to better simulate rough surfaces and partially vegetated surfaces. The *b* parameter was given a value of 0.034 for the tree-soil summer period, based on the range reported in Sauer et al. (1995) for partial vegetation conditions (Kustas et al. 2016; Sauer et al., 1995). Other parameters, such as χ_{LAD}, which is presumably different between grasses and trees, were not modified since they showed little sensitivity (Fig. 5)

To improve the seasonal depiction and related changes to the ecosystem, the TSEB model was adapted using a two-season modeling approach (TSEB-2S) as proposed in section 2.4.4. The simulation period was divided into two main phenological periods where a dominant vegetation is assumed in each case and TSEB is parameterized according to the respective end-member parameter values shown in table 4 (i.e. $TSEB_{grass}$ during the growing season and $TSEB_{tree}$ during the dry summer)

485

Table 4. $TSEB_{grass}$ and $TSEB_{tree}$ model configurations based on global SA

Parameters	End-Member	
	$TSEB_{grass}$	$TSEB_{tree}$
α_{PT} (-)	1.26	1.26
f_g (-)	0.7	0.9
f_c (-)	1	0.2
w_c (-)	1	1
X_{LAD} (-)	1	1
h_c (m)	0.5	8
$z0_{soil}$ (m)	0.01	0.01
l_w (m)	0.01	0.05
b (-)	0.012	0.034
c ($m\ s^{-1}\ K^{-1/3}$)	0.0025	0.0025
C' ($s^{1/2}\ m^{-1}$)	90	90

3.3 Model evaluations for main simulation period (2015 CT)

490 Fig 7 shows the modeled vs. observed half hourly turbulent fluxes as well as the annual trend of daytime average sensible heat flux, both modeled and observed. Model results of TSEB-DF vastly underestimate H (bias: -39 W m^{-2}) and, consequently, overestimate LE (bias: 34 W m^{-2}) as compared with observed EC data. As shown in Fig. 7 (left panel), high errors are observed throughout (RMSD of H: 76 W m^{-2}) but errors stem particularly from the very large underestimations of H during the hot and dry summer period (Fig.7, right panel).

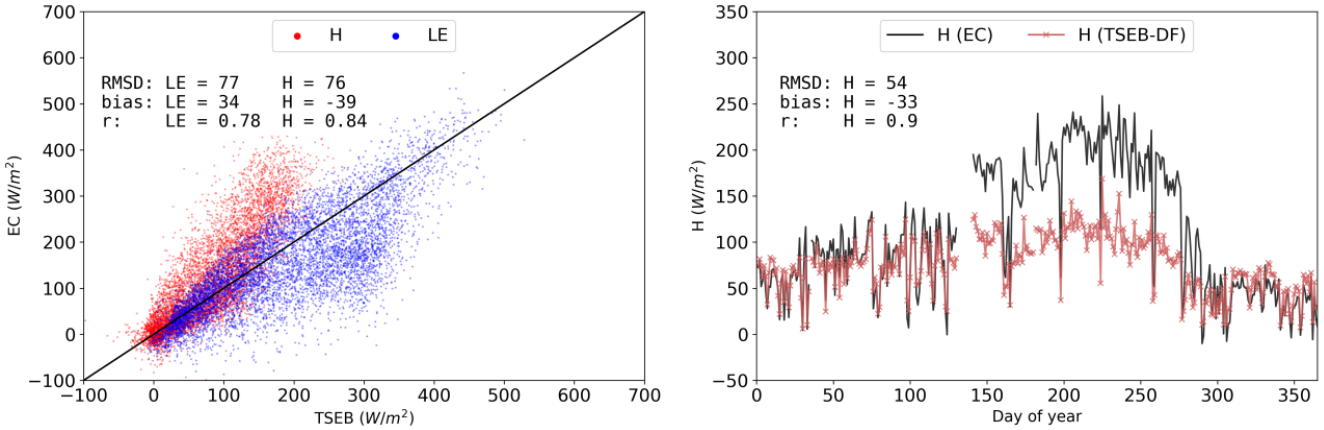

Figure 7. Observed vs modeled daytime half-hourly H (red) and LE (blue) density scatterplot (left) and time series of simulated (red) and observed (black) daytime daily mean H (right) for $TSEB_G$-DF in 2015 at CT

The end member simulations demonstrate the 'boundary conditions' when the simulations completely ignore one of the vegetation layers throughout the year (Fig. 8). Predictably, $TSEB_{grass}$ overestimates LE even more than TSEB-DF (bias: 48 W m^{-2}), while, by contrast, LE is largely underestimated in $TSEB_{tree}$ (bias:-23 W m^{-2}), with large errors (RMSD: 82 W m^{-2})

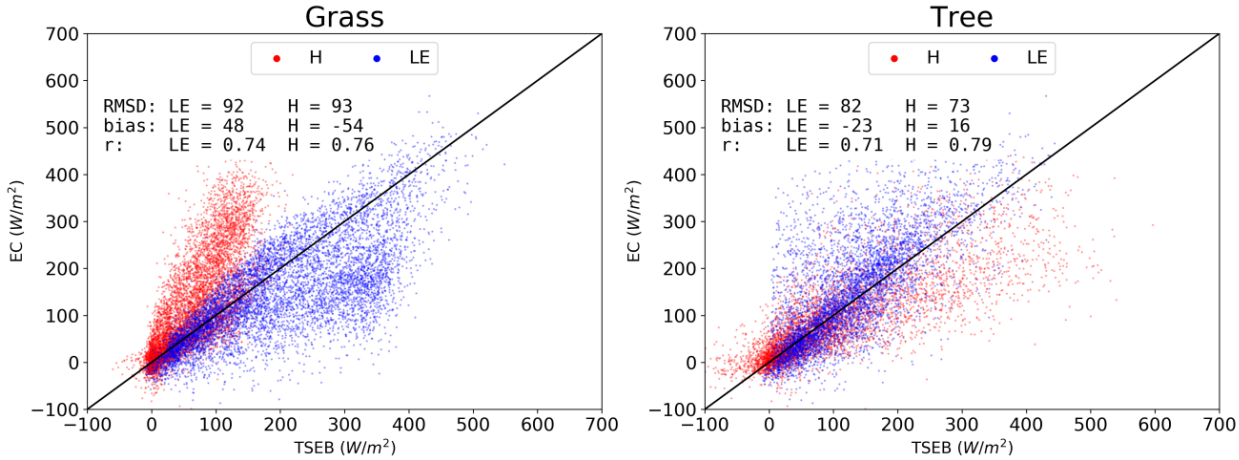

Figure 8. Observed vs modeled half-hourly daytime H (red) and LE (blue) density scatterplot for $TSEB_{grass}$ (left) and $TSEB_{tree}$ (right) for 2015 at CT

The performance of the proposed TSEB-2S parameterization is shown in Fig. 9 where the simulation of LE and H for 2015 improved considerably when using TSEB-2S compared to TSEB-DF. By comparing Fig.7 and Fig.9, errors with TSEB-2S decrease substantially (decrease in RMSD from 77 W m^{-2} and 76 W m^{-2} to 59 W m^{-2} and 56 W m^{-2} for LE and H, respectively) and the seasonal average daily H is much improved, particularly during the summer/dry period (RMSD of daily

mean H decreased from 54 W m^{-2} to 28 W m^{-2}). However, the winter-autumn period (roughly between DOY 25 and 125) showed a slight systematic H underestimation with TSEB-2S.

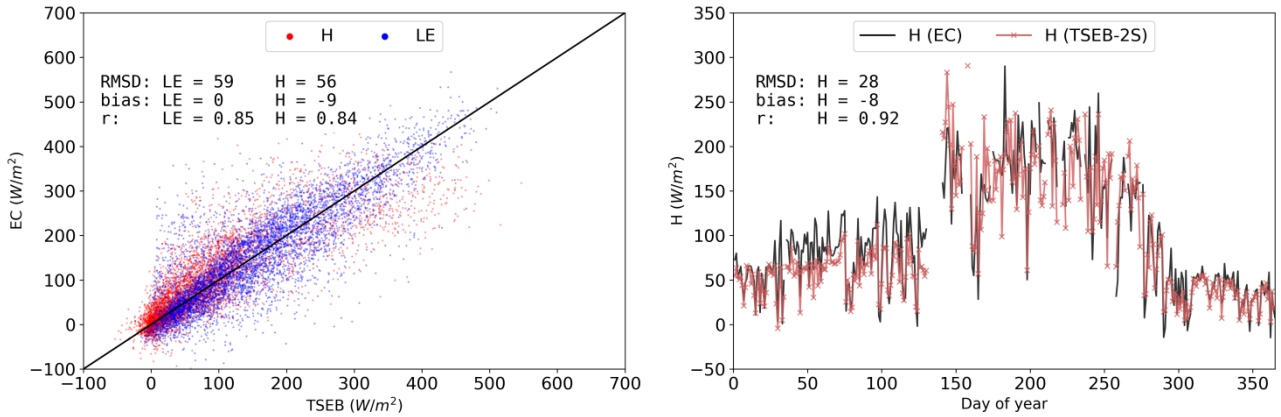

Figure 9. Observed vs modeled daytime half-hourly H (red) and LE (blue) density scatterplot (left) and time series of simulated (red) and observed (black) daytime daily mean H (right) for TSEB-2S simulations of 2015 at CT

3.4 TSEB-2S Validation

3.4.1 Independent spatial and temporal evaluation

TSEB-2S was additionally tested for all EC towers (CT, NT and NPT) in 2016 and 2017. The results from the other towers and years (Fig. 10) were within similar error ranges to the benchmark TSEB-2S 2015 simulation at the CT. RMSD for LE ranges between 51 and 63 W m^{-2} for all the different simulations. In general, results for the year 2016 had a slightly greater overestimation of LE (bias between 6 and 17 W m^{-2}) while the bias in the 2017 simulations were much more aligned to the observed data (between 0 and -3 W m^{-2}).

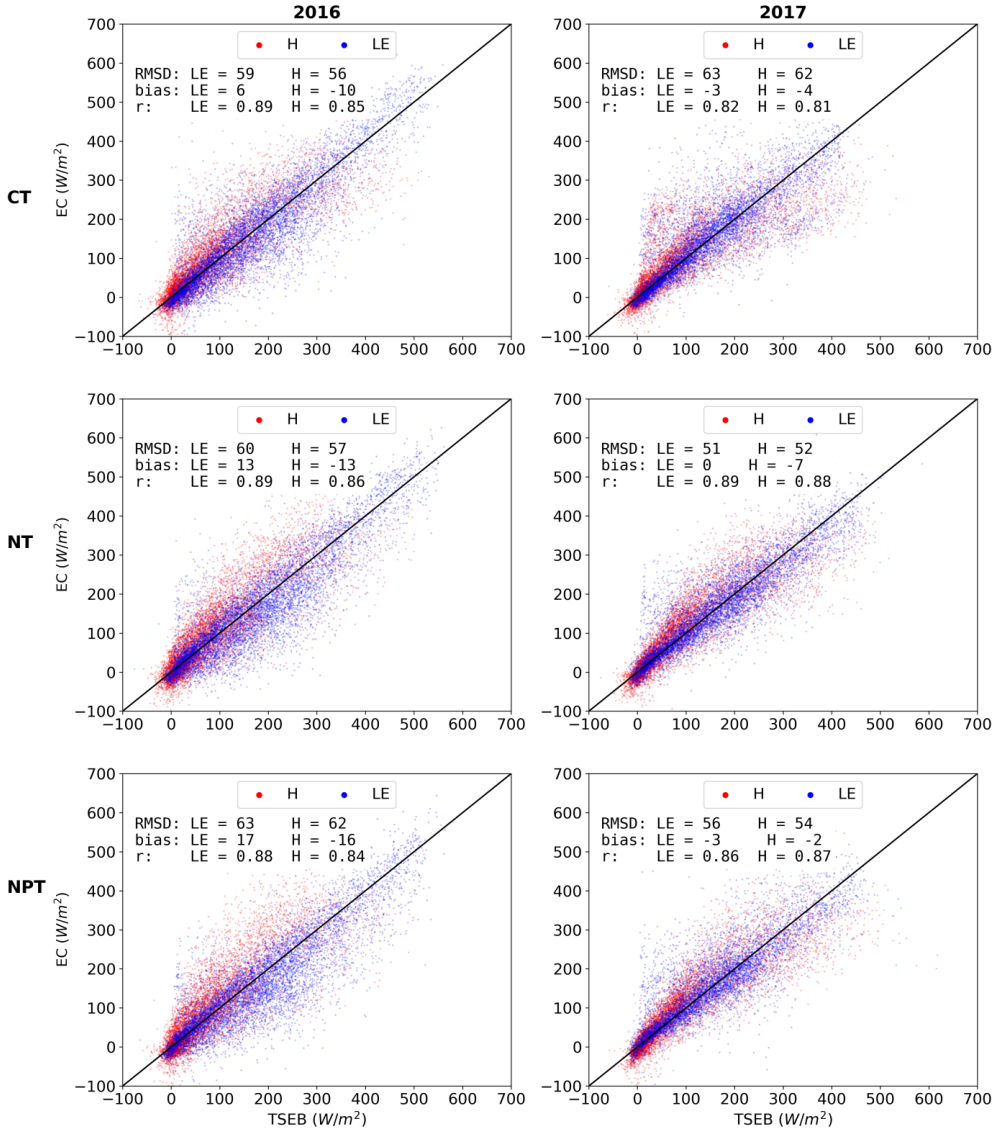

Figure 10. Observed vs modelled daytime half-hourly H (red) and LE (blue) density scatterplot for TSEB-2S for CT, NT and NPT; and years 2016 (left column) and 2017 (right column).

3.4.2 LE partitioning

The LE partitioning in TSEB-2S was evaluated against independent estimates from the lysimeter at the CT footprint during the summer drought, when there is no grass transpiration and, thus, LE measured by the lysimeter (LE_{lys}) corresponds to soil evaporation (Perez-Priego et al., 2018, 2017). It was additionally compared against an EC LE partitioning method (Perez-Priego et al., 2018). Results indicate a systematic LE_s underestimation during the dry period for the three years analyzed (Fig. 9). The LE_s underestimation was largest for 2017 (bias: -22 W m^{-2}). Errors (i.e RMSD) were largest for 2016 due mostly to greater variability, or short term fluctuations, observed in modeled results compared to the relatively stable

lysimeter measurements. As shown in Fig. 11, TSEB-2S showed largest underestimation during the dry down period (roughly DOY170-185) but was able to capture the evaporation peaks relatively well caused by the rare summer precipitation events in 2016 and 2017.

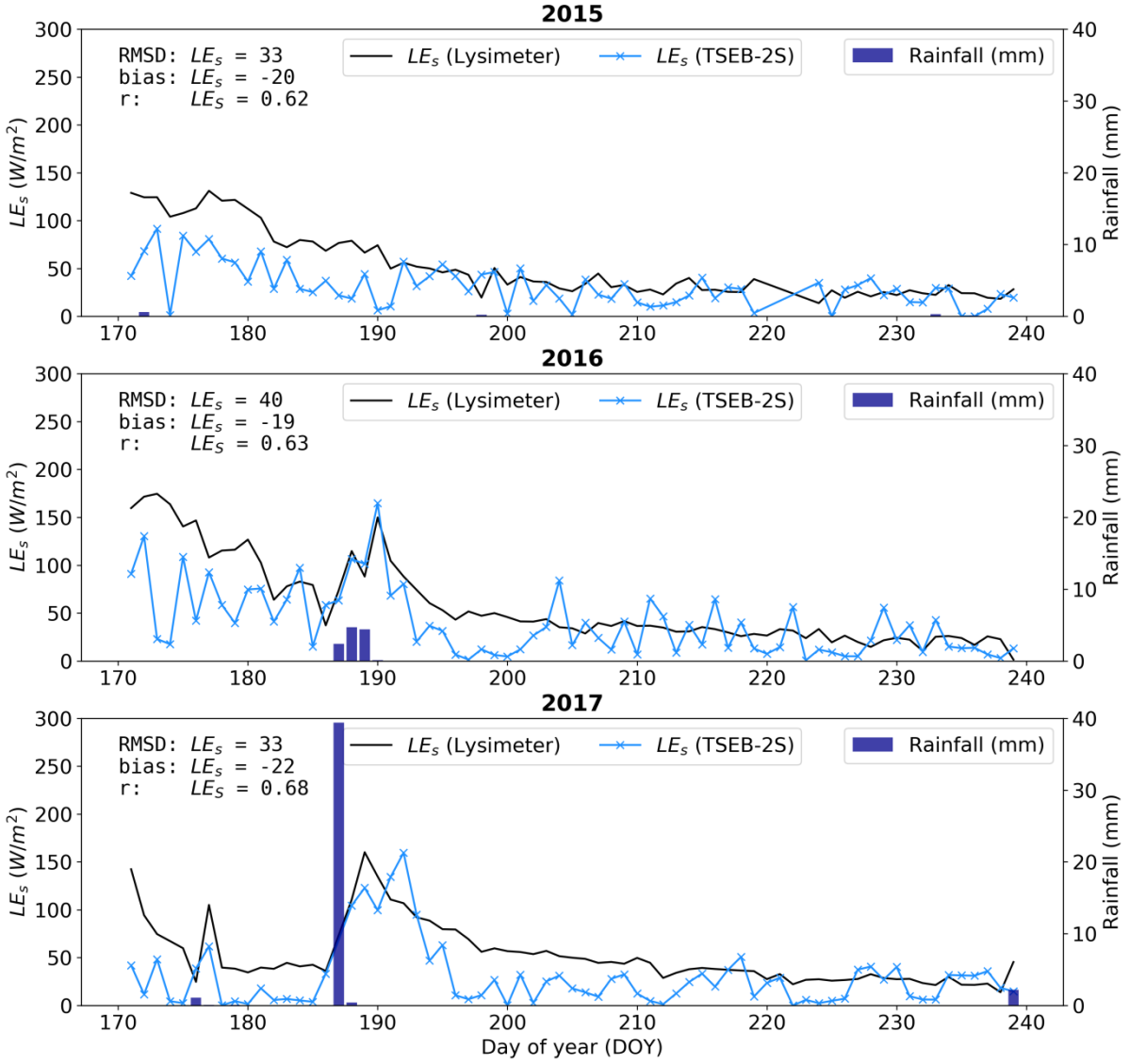

Figure 11. Time series of simulated (blue) and observed (black) daytime daily mean LE_s at CT during the peak summer in 2015, 2016 and 2017 using TSEB-2S. LE measured by the lysimeter is assumed to be equivalent to LE_s during the summer period due to grass senescence

The LE_s underestimation, and thus LE_c overestimation, was also supported when comparing canopy transpiration estimates from TSEB-2S with transpiration estimates based on Perez-Priego et al. (2018) ($LE_{c,PP}$) (Fig. 12). Throughout most of the year, modeled LE_c had a very important positive bias compared to $LE_{c,PP}$. However, during the dry period, LE_c from TSEB-2S was more closely in line with $LE_{c,PP}$ although a bias maintained noticeable (Fig. 12). Since $LE_{c,PP}$ contained both tree and grass contribution, the $LE_{c,PP}$ peak was more sustained than LE_c from TSEB-2S. This is explained by the successive influence of the grass (DOY~90) followed by the trees in late-May/early-June (DOY~150), then a gradual decline during the dry-down as modulated by water stress. By contrast, TSEB-2S modeled LE_c peaks earlier, around late-April, and proceeds to decline very rapidly when summer begins, coinciding with the change in model configuration between the grass-soil to the tree-soil system. LE_c from TSEB-2S also showed an important increase in the re-greening phase (~ September to late-October; DOY~250 to DOY~300), which was less pronounced in $LE_{c,PP}$. It should be noted that is merely a comparison and not an evaluation/validation, as $LE_{c,PP}$ is not an observed data series, but an transpiration estimation based on the method of Perez-Priego et al. (2018)

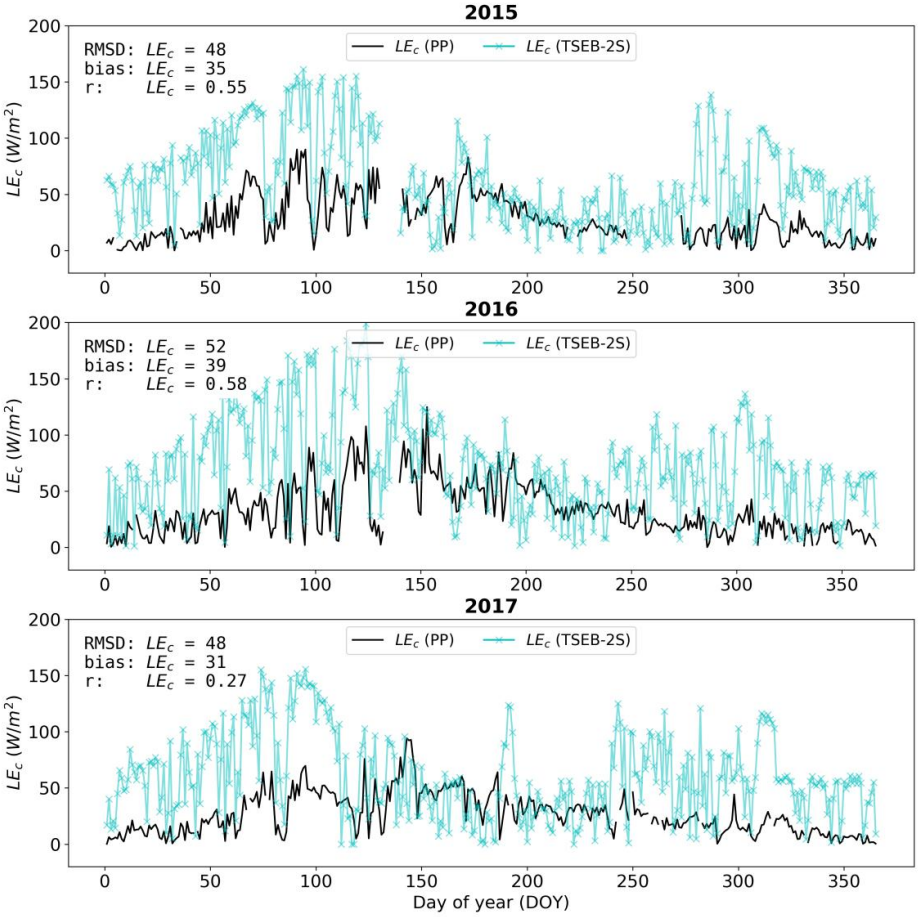

Figure 12. Annual time series of daytime daily mean TSEB-2S simulated LE_c (blue) and estimated $LE_{c,PP}$ (black) at CT in years 2015, 2016 and 2017

4. Discussion

The proposed TSEB-2S vastly improved model performance in simulating LE and H compared to the default TSEB configuration (RMSD and bias of modeled H decreases from 76 and -39 W m^{-2} to 56 and -9 W m^{-2}, respectively). The simple assumption of two separate phenological and modeling periods, one dominated by a grass-soil system and the other dominated by a tree-soil system, allowed for a two-layer model to accurately simulate turbulent energy fluxes in an essentially three (tree-grass-soil) layer ecosystem. TSEB assumes only one vegetated layer, being more or less photosynthetically active, over a non-photosynthetically active layer (i.e. bare soil or similar) and, as such, it becomes difficult to properly parameterize the model when numerous vegetation covers are simultaneously present. Additionally, as in the case of many TGEs, the influence of the grass understory changes throughout the year, where it becomes largely non-photosynthetically active (i.e. not transpiring) during the summer. Therefore, these vastly different seasonal conditions and characteristics were better captured using TSEB-2S, by assuming a 'dominant' vegetation cover for different phenological periods, compared to the default, non-seasonally changing, configuration of TSEB.

The results also demonstrate that large changes to the vegetated surface have a considerable influence on the surface energy balance. This confirms the importance of vegetation characteristics in controlling and mediating ecosystem level energy fluxes, where seasonal dynamics and phenology of vegetation are key considerations for land-atmospheric modeling. The TSEB-2S model demonstrated robustness, being able to accurately simulate different intra-annual dynamics for various years and towers with differing surface conditions from the nutrient fertilization experiment (Fig. 10). The relatively simple and automatic separation of seasons from a MODIS-NDVI time series can easily be extrapolated to other TGEs or similar temporally dynamic sites, as these data are globally available. Results and the associated magnitudes of errors for all TSEB-2S model runs are similar to the error bounds found in other energy balance model studies (e.g. Andreu et al., 2018; Boulet et al., 2015; Gan and Gao, 2015; Gonzalez-Dugo et al., 2009; Guzinski et al., 2014; Kustas et al., 2016; Kustas and Norman, 1999; Timmermans et al., 2007) and close to the typical uncertainty of surface turbulent flux measurement systems (i.e. ~50 W m^{-2}; Kustas and Norman, 2000). For instance, RMSD of LE between 62 and 70 W m^{-2} were achieved in Timmermans et al. (2007), who compared the use of TSEB against a one-source energy balance model for a sparsely vegetated grassland and rangeland. In Boulet et al. (2015), different dual-source model schemes were tested and obtained an RMSD between 53 and 73 W m^{-2} for midday instantaneous LE for both irrigated and rainfed wheat fields. Therefore, results presented here, are in line with past studies related to LE retrievals with energy balance models, with these considering much more homogeneous land cover types. Andreu et al. (2018) applied various modified versions of TSEB, notably with different wind profiles and roughness schemes, in similarly complex TGEs and reported errors between 44 and 60 W m^{-2} for simulated LE. These are comparable to the error bounds presented here even though quite different approaches were used for these complex TGEs. In this study, the basic TSEB model structure was not modified, instead opting to alter the model parameterization depending on the phenological period using typical land cover characteristics (i.e. grasslands and evergreen broadleaved trees). This way, the approach applied here is less local and may be applicable for different sites and ecosystems with similar

heterogeneous features and phenology. As such, the findings here may complement the methods used in Andreu et al. (2018), who also reported largest errors during the dry, summer period. This work additionally investigated the partitioning of LE, which is a complex process to separate in ecosystems that have multiple vegetation layers.

The global SA demonstrated that TSEB was most sensitive to f_c. This is largely due to f_c being a key input to estimate the Ω (Kustas and Norman, 1999), which in turn affects the radiation interception and partitioning between the mixed vegetated and soil surfaces. The estimation of Ω is mostly based on the transmission through the vegetated layer where f_c is used to obtain a local LAI (LAI/f_c) and as an important weighting factor for the gap fraction estimation (section 2.2.1). These results are largely in line with results from Li et al. (2005), who found that the Ω uncertainties had a large impact on flux outputs from TSEB. They tested incremental f_c values, between 0.1 and 1, that resulted in sharp H changes, particularly between higher f_c values, an indication of a high sensitivity for this parameter. The f_g was found to be more sensitive compared to α_{PT} even though both parameters are part of the initial canopy transpiration estimate from the Priestly-Taylor formulation (eq. 7). This is the case since the latter is merely an initial value and is iteratively changed through the modeling scheme, if the resulting soil evaporation flux is unrealistic. The b coefficient was the only more empirically derived parameter that demonstrated relatively large influence. In addition, the input SA showed that uncertainties in LST and LAI both translate into uncertainties in modeled H. Gan and Gao (2015) also found TSEB to be sensitive to biases in LST, where a 1K change is associated with median daily ~12 - 25 W m^{-2} bias. A local LAI SA in Li et al. (2005) added +-20% deviation to LAI and investigated the associated relative H change in TSEB. Their associated ~3-8% bias in modeled H is similar to the results presented here, with a 20% change in LAI being associated with a median H bias of 6.1% with TSEB-DF. As such, the more comprehensive SA analysis presented here, taking into account parameter interaction in the global SA combined with a local input SA, were largely in line with results presented in different local and parameter specific SAs from the literature. This is indicative that these results will be useful for future studies, as we quantified the different sources of uncertainty and relative influence of the different modeling components in TSEB, which may also be useful for other similar thermal-based energy balance models.

As shown, bulk (soil + vegetation) fluxes were well modeled in TSEB-2S for different years and towers. However, the partitioning of LE, between LE_s and LE_c, had greater uncertainty, with biases observed compared to the lysimeter measurements (Fig. 11) and compared to a physiologically-based EC partitioning method (Fig. 12). Since total LE was well modeled, this indicates errors associated with the partitioning itself. Against summer measurements of the lysimeter, LE_s were consistently underestimated by TSEB-2S. This may be due to TSEB interpreting moderately stressed vegetation with a moist soil as fully transpiring vegetation with a dry soil. The partition of LE is largely controlled through LAI within TSEB (Kustas et al., 2019), as evident in how the LE_c time series (Fig. 9) roughly follows the trend of the LAI input time series shown in Fig. 4. The rapid decrease in LAI as the summer begins results in a rapid change in TSEB-2S derived LE_c, in contrast to the gradual decrease of $LE_{c,PP}$. This can also be attributed to TSEB-2S´s sudden change in model configuration

(i.e. from grass to tree dominated). The transition periods between the two modeling periods had the largest biases (roughly around DOY 120 and DOY 300) as the model configuration does not consider gradual changes to f_g or other parameters, while the summer period, when the model considers only the tree-soil system, produced the best simulated LE partitions. The poor performance in the LE partitioning may be linked to the assumed vegetation cover of the two different seasons not properly depicting the complex vegetation characteristics observed, notably during the growing season when the tree layer is neglected. TSEB's relatively poor performance in partitioning LE was also observed over a vineyard in Kustas et al. (2019). However, Xu et al. (2016) reported a relatively good performance of TSEB's midday LE partitioning over an irrigated cropland against observations using the isotope approach. Colaizzi et al. (2014) demonstrated that using the Penman-Monteith equation to derive initial canopy transpiration in TSEB resulted in a better agreement with LE_s and LE_c compared to the Priestley-Taylor approach. Colaizzi et al. (2014) also reported the strong influence of vapour pressure deficit over LE_c in an irrigated cotton field within an advective, semi-arid climate, which was captured most successfully using the Penman-Monteith approach. As stated in Kustas et al. (2019), more studies need to evaluate whether the poor partitioning is linked to uncertainties in input values (i.e LAI) or biases caused by the modeling structure itself (i.e. initial potential canopy transpiration, radiation transfer).

As demonstrated, a simple adaptation to the modeling scheme within TSEB, depicting the seasonal changes in the ecosystem, were able to successfully simulate LE and H in a complex ecosystem. However, certain limitations are still present including the slight systematic underestimation of H during the grass growing season, particularly visible in the 2015 daily H time series (Fig. 9). This is likely due to the modeling scheme in this period ignoring the effect of the tree canopy layer on the turbulent transport and hence on the calculation of the aerodynamic resistances. Compared to grasslands, tree canopies are more aerodynamically coupled to the atmosphere and hence their aerodynamic resistance is lower, resulting in that trees can dissipate heat more efficiently (El-Madany et al., 2018). As discussed in El-Madany et al. (2018), tree canopies in the Majadas experimental site were an additional H source, even though they tend to have a lower LST than the grass layer. As such, ignoring the tree canopy during the growing periods may not adequately represent the turbulent transport characteristics of the ecosystem resulting in H underestimations, in some cases. Neglecting the tree canopy during the growing season is also a reason for the greater bias in LE partitioning during the growing season (Fig. 12), as underestimations in H translate into greater available energy for LE residual. Further adaptations to the TSEB model may be needed for the more operational and larger scale use of this model, notably for similarly complex ecosystems such as TGEs. The differences between soil, grass and tree layers should inherently be integrated within the modeling structure to robustly consider their different geometric, physical and phenological properties and their resulting effect on energy fluxes. This was also hinted in Andreu et al. (2018), who incorporated different layers in a modified Goudriaan (1977) wind speed profile scheme to consider differences between tree and grass canopy layers for TGEs.

5. Conclusions

When accounting for different phenological periods, the TSEB model provided robust LE and H estimations for a three-layered heterogeneous and semi-arid TGE. This confirms the important role that vegetation characteristics, notably its structure (i.e. h_c) and cover (i.e. f_c and f_g), have on ecosystem level energy fluxes. The f_c was the single most influential parameter on model performance, largely due to its role in characterizing vegetation clumping and how this, in turn, interacts significantly with other parameters. In addition, the uncertainties related to the traditionally remotely sensed derived inputs, notably LST, showed an important influence on output uncertainties.

The LE partitioning, between canopy and soil, showed larger bias compared to the bulk fluxes, particularly during the transition towards the grass senescence period and the prominent contribution of the tree layer. Based on this, further research should focus on the understanding of the radiation partitioning between the canopy and soil layers, and, particularly, inherently accounting for the important differences between soil, grass and tree layers of TGEs within the modeling structure.

Author contribution

All authors contributed to discussing and improving the manuscript. MPM, HN, DR and VBL designed and formulated the research. MM and AC designed the experimental infrastructure. VBL analyzed the data, created the figures and wrote the manuscript. AC, MM, TSEM collected eddy covariance and biomet data. OPP collected, processed and provided lysimeter data. MPM sampled and analyzed field LAI samples.

The authors declare that they have no conflict of interest.

Code and Data Availability

EC, meteo and in-situ biophysical measurement data necessary to run and evaluate model results are available via the online repository (*link to Zenondo repository*). The python script of the two-source energy balance model (TSEB) is freely available via the link https://github.com/hectornieto/pyTSEB. The sensitivity analysis was performed using the Sensitivity Analysis Library (SALib) package in python, which is available via the link https://github.com/SALib/SALib.The ET partitioning code, as described in Perez-Priego et al. (2018), is implemented in R (R Development Core Team, 2010) and freely available via the link https://github.com/oscarperezpriego/ETpartitioning.

Acknowledgements

The project has received funding from the European Union's Horizon 2020 research and innovation programme under the Marie Sklodowska-Curie grant agreement No 721995.

This research was also funded by Ministerio de Economía y Competitividad through FLUXPEC CGL2012-34383 and SynerTGE CGL2015-G9095-R (MINECO/FEDER, UE) projects.

The research infrastructure at the measurement site Majadas de Tiétar was partly funded through the Alexander von Humboldt Foundation.

685

690

5. References

Alfieri, J.G., Kustas, W.P., Nieto, H., Prueger, J.H., Hipps, L.E., McKee, L.G., Gao, F., and Los, S.: Influence of wind direction on the surface roughness of vineyards, Irrigation Sci., 37, 359–373, https://doi.org/10.1007/s00271-018-0610-z, 2019.

Allen, R., Tasumi, M., and Trezza, R.: Satellite-Based Energy Balance for Mapping Evapotranspiration with Internalized Calibration (METRIC) — Model, J. Irrig. Drain. Eng., 133, 380–394. https://doi.org/10.1061/(ASCE)0733-9437(2007)133:4(380), 2007.

Anderson, M.C., Norman, J.M., Kustas, W.P., Li, F., Prueger, J.H., and Mecikalski, J.R.: Effects of vegetation clumping on two–source model estimates of surface energy fluxes from an agricultural landscape during SMACEX, J. Hydrometeorol., 6, 892–909. 2005.

Andreu, A., Kustas, W., Polo, M., Carrara, A., and González-Dugo, M.: Modeling Surface Energy Fluxes over a Dehesa (Oak Savanna) Ecosystem Using a Thermal Based Two-Source Energy Balance Model (TSEB) I, Remote Sensing, 10(4), 567. https://doi.org/10.3390/rs10040567, 2018.

Baldocchi, D.D., Xu, L., and Kiang, N.: How plant functional-type, weather, seasonal drought, and soil physical properties alter water and energy fluxes of an oak–grass savanna and an annual grassland, Agricultural and Forest Meteorology, 123, 13–39, 2004.

Bastiaanssen, W., Menenti, M., Feddes, R., and Holtslag, A.: A remote sensing surface energy balance algorithm for land (SEBAL). 1. Formulation, Journal of Hydrology, 212, 198–212, 1998.

Beven, K.: Changing ideas in hydrology — The case of physically-based models, Journal of Hydrology, 105, 157–172. https://doi.org/10.1016/0022-1694(89)90101-7, 1989.

Bonan, G.B., and Doney, S.C.: Climate, ecosystems, and planetary futures: The challenge to predict life in Earth system models, Science, 359 (6375), eaam8328. https://doi.org/10.1126/science.aam8328, 2018.

Boulet, G., Mougenot, B., Lhomme, J.-P., Fanise, P., Lili-Chabaane, Z., Olioso, A., Bahir, M., Rivalland, V., Jarlan, L., Merlin, O., Coudert, B., Er-Raki, S., and Lagouarde, J.-P.: The SPARSE model for the prediction of water stress and evapotranspiration components from thermal infra-red data and its evaluation over irrigated and rainfed wheat, Hydrol. Earth Syst. Sc., 19, 4653–4672. https://doi.org/10.5194/hess-19-4653-2015, 2015.

Campbell, G.S., and Norman, J.M..: An Introduction to Environmental Biophysics, 2nd Edition, ed. Springer-Verlag New York, New York, 1998.

Casals, P., Gimeno, C., Carrara, A., Lopez-Sangil, L., and Sanz, Mj.: Soil CO2 efflux and extractable organic carbon fractions under simulated precipitation events in a Mediterranean Dehesa, Soil Biology and Biochemistry, 41, 1915–1922. https://doi.org/10.1016/j.soilbio.2009.06.015, 2009.

Colaizzi, P.D., Agam, N., Tolk, J.A., Evett, S.R., Howell Sr, T.A., O'Shaughnessy, S.A., Gowda, P.H., Kustas, W.P., and Anderson, M.C.: Advances in a two-source energy balance model: Partitioning of evaporation and transpiration for cotton, Transactions of the ASABE 59, 181–197, 2016.

Colaizzi, P.D., Agam, N., Tolk, J.A., Evett, S.R., Howell, T.A., Gowda, P.H., O'Shaughnessy, S.A., Kustas, W.P., and Anderson, M.C.: Two-source energy balance model to calculate E, T, and ET: Comparison of Priestley-Taylor and Penman-Monteith formulations and two time scaling methods. Transactions of the ASABE 57, 479–498, 2014.

Colaizzi, P.D., Evett, S.R., Howell, T.A., and Tolk, J.A.: Comparison of aerodynamic and radiometric surface temperature using precision weighing lysimeters, Remote sensing and modeling of ecosystems for sustainability, 5544, 215-230, International Society for Optics and Photonics. https://doi.org/10.1117/12.559503, 2004.

Diarra, A., Jarlan, L., Er-Raki, S., Le Page, M., Aouade, G., Tavernier, A., Boulet, G., Ezzahar, J., Merlin, O., and Khabba, S.: Performance of the two-source energy budget (TSEB) model for the monitoring of evapotranspiration over irrigated annual crops in North Africa, Agricultural Water Management, 193, 71–88. https://doi.org/10.1016/j.agwat.2017.08.007, 2017.

El-Madany, T.S., Reichstein, M., Carrara, A., Perez-Priego, O., Martín, M.P., Moreno, G., Martín, M.P., Pacheco-Labrador, J., Wohlfahrt, G., Nieto, H., Weber, U., Kolle, O., Luo, Y.-P., Carvalhais, N., and Migliavacca, M.: Drivers of spatio-temporal variability of carbon dioxide and energy fluxes in a Mediterranean savanna ecosystem, Agricultural and Forest Meteorology, 262, 258–278. https://doi.org/10.1016/j.agrformet.2018.07.010, 2018.

El-Madany, T.S., Reichstein, M., Carrara, A., Martín, M.P., Moreno, G., González-Cascón, R., Peñuelas, J., Burchard-Levine, V., Hammer, T., Knauer, J., Kolle, O., Luo, Y.P., Pacheco-Labrador, J., Perez-Priego, O., Rolo, V., Wutzler, T., and Migliavacca, M.: Rapid shifts of ecosystem carbon and energy fluxes after nitrogen and phosphorus availability, in preperation.

Foken, T., Aubinet, M., Finnigan, J.J., Leclerc, M.Y., Mauder, M., and Paw U, K.T.: Results of a panel discussion about the energy balance closure correction for trace gases. Bulletin of the American Meteorological Society, 92, ES13–ES18, 2011.

Friedl, M.A., Sulla-Menashe, D., Tan, B., Schneider, A., Ramankutty, N., Sibley, A., and Huang, X.: MODIS Collection 5 global land cover: Algorithm refinements and characterization of new datasets, Remote Sens. Environ., 114, 168–182, 2010.

Gan, G., and Gao, Y.: Estimating time series of land surface energy fluxes using optimized two source energy balance schemes: Model formulation, calibration, and validation, Agricultural and forest meteorology, 208, 62–75, 2015.

García, M., Gajardo, J., Riaño, D., Zhao, K., Martín, P., and Ustin, S.: Canopy clumping appraisal using terrestrial and airborne laser scanning, Remote Sens. Environ., 161, 78–88, 2015.

Gonzalez-Dugo, M.P., Neale, C.M.U., Mateos, L., Kustas, W.P., Prueger, J.H., Anderson, M.C., and Li, F.: A comparison of operational remote sensing-based models for estimating crop evapotranspiration, Agricultural and Forest Meteorology, 149, 1843–1853, 2009

Goudriaan, J.: Crop Micrometeorology: A Simulation Study, Center for Agricultural Publications and Documentation, Wageningen, 1977.

Guzinski, R., Anderson, M.C., Kustas, W.P., Nieto, H., and Sandholt, I.: Using a thermal-based two source energy balance model with time-differencing to estimate surface energy fluxes with day-night MODIS observations. Hydrol. Earth Syst. Sc., 17, 2809–2825, 2013.

Guzinski, R., Nieto, H., Jensen, R., Mendiguren, G.: Remotely sensed land-surface energy fluxes at sub-field scale in heterogeneous agricultural landscape and coniferous plantation. Biogeosciences, 11, 5021–5046, 2014

Herman, J. and Usher, W.: SALib: An open-source Python library for sensitivity analysis. Journal of Open Source Software, 2, 9, doi:10.21105/joss.00097, 2017.

Jasechko, S., Sharp, Z.D., Gibson, J.J., Birks, S.J., Yi, Y., and Fawcett, P.J.: Terrestrial water fluxes dominated by transpiration, Nature, 496, 347, 2013

Jin, X., Xu, C.-Y., Zhang, Q., and Singh, V.P.: Parameter and modeling uncertainty simulated by GLUE and a formal Bayesian method for a conceptual hydrological model, Journal of Hydrology, 383, 147–155. https://doi.org/10.1016/j.jhydrol.2009.12.028, 2010.

Jung, M., Henkel, K., Herold, M., Churkina, G.: Exploiting synergies of global land cover products for carbon cycle modeling, Remote Sens. Environ., 101, 534–553. https://doi.org/10.1016/j.rse.2006.01.020, 2006.

Kalma, J.D., McVicar, T.R., and McCabe, M.F.: Estimating Land Surface Evaporation: A Review of Methods Using Remotely Sensed Surface Temperature Data, Surv. Geophys., 29, 421–469. https://doi.org/10.1007/s10712-008-9037-z, 2008.

Kljun, N., Calanca, P., Rotach, M.W., and Schmid, H.P.: A simple two-dimensional parameterisation for Flux Footprint Prediction (FFP). Geosci. Model Dev., 8, 3695–3713. https://doi.org/10.5194/gmd-8-3695-2015, 2015.

Kondo, J., and Ishida, S.: Sensible Heat Flux from the Earth's Surface under Natural Convective Conditions, J. Atmos. Sci., 54, 498–509, 1997.

Krinner, G., Viovy, N., de Noblet-Ducoudré, N., Ogée, J., Polcher, J., Friedlingstein, P., Ciais, P., Sitch, S., and Prentice, I.C.: A dynamic global vegetation model for studies of the coupled atmosphere-biosphere system, Global Biogeochemical Cycles, 19(1), https://doi.org/10.1029/2003GB002199, 2005.

Kustas, W.P., Alfieri, J.G., Anderson, M.C., Colaizzi, P.D., Prueger, J.H., Evett, S.R., Neale, C.M., French, A.N., Hipps, L.E., and Chávez, J.L.: Evaluating the two-source energy balance model using local thermal and surface flux observations in a strongly advective irrigated agricultural area, Advances in Water Resources, 50, 120–133, 2012.

Kustas, W.P., Alfieri, J.G., Nieto, H., Wilson, T.G., Gao, F., and Anderson, M.C., 2019, Utility of the two-source energy balance (TSEB) model in vine and interrow flux partitioning over the growing season, Irrig. Sci., 37, 375–388. https://doi.org/10.1007/s00271-018-0586-8, 2019

Kustas, W.P., and Anderson, M.C.: Advances in thermal infrared remote sensing for land surface modeling, Agricultural and Forest Meteorology, 149, 2071–2081, 2009.

Kustas, W.P., Nieto, H., Morillas, L., Anderson, M.C., Alfieri, J.G., Hipps, L.E., L.Villagarcía, Domingo, F., and García, M.: Revisiting the paper "Using radiometric surface temperature for surface energy flux estimation in Mediterranean drylands from a two-source perspective", Remote Sens. Environ., 184, 645–653, 2016.

Kustas, W.P., and Norman, J.M.: Evaluation of soil and vegetation heat flux predictions using a simple two-source model with radiometric temperatures for partial canopy cover, Agricultural and Forest Meteorology, 94, 13–29, 1999.

Kustas, W.P., and Norman, J.M.: Evaluating the Effects of Subpixel Heterogeneity on Pixel Average Fluxes, Remote Sens. Environ., 74, 327–342, 2000.

Li, F., Kustas, W.P., Prueger, J.H., Neale, C.M., and Jackson, T.J.: Utility of remote sensing–based two-source energy balance model under low-and high-vegetation cover conditions, J. Hydrometeorol., 6, 878–891, 2005.

LICOR Bioscience USA: LAI-2200 Plant Canopy Analyzer, Instruction Manual, 2011.

Lindroth, A.: Aerodynamic and canopy resistance of short-rotation forest in relation to leaf area index and climate, Boundary-Layer Meteorology, 66, 265–279, 1993.

Luo, Y., El-Madany, T., Filippa, G., Ma, X., Ahrens, B., Carrara, A., Gonzalez-Cascon, R., Cremonese, E., Galvagno, M., and Hammer, T.: Using Near-Infrared-Enabled Digital Repeat Photography to Track Structural and Physiological Phenology in Mediterranean Tree–Grass Ecosystems, Remote Sensing, 10, 1293, 2018.

Massman, W.J., Forthofer, J.M., Finney, M.A.: An improved canopy wind model for predicting wind adjustment factors and wildland fire behavior, Canadian Journal of Forest Research, 47, 594–603, https://doi.org/10.1139/cjfr-2016-0354, 2017.

McNaughton, K.G., and Van Den Hurk, B.J.J.M.: A "Lagrangian" revision of the resistors in the two-layer model for calculating the energy budget of a plant canopy, Boundary-Layer Meteorology, 74, 261–288, 1995.

Mendiguren, G., Pilar Martín, M., Nieto, H., Pacheco-Labrador, J., and Jurdao, S.: Seasonal variation in grass water content estimated from proximal sensing and MODIS time series in a Mediterranean Fluxnet site, Biogeosciences, 12, 5523–5535, 2015

Migliavacca, M., Perez-Priego, O., Rossini, M., El-Madany, T.S., Moreno, G., van der Tol, C., Rascher, U., Berninger, A., Bessenbacher, V., and Burkart, A.: Plant functional traits and canopy structure control the relationship between photosynthetic CO 2 uptake and far-red sun-induced fluorescence in a Mediterranean grassland under different nutrient availability, New Phytologist, 214, 1078–1091, 2017.

Migliavacca, M., Sonnentag, O., Keenan, T.F., Cescatti, A., O'Keefe, J., Richardson, A.D., 2012. On the uncertainty of phenological responses to climate change, and implications for a terrestrial biosphere model. Biogeosciences 9, 2063–2083. https://doi.org/10.5194/bg-9-2063-2012, 2012.

Nieto, H., Kustas, W.P., Alfieri, J.G., Gao, F., Hipps, L.E., Los, S., Prueger, J.H., McKee, L.G., and Anderson, M.C.: Impact of different within-canopy wind attenuation formulations on modelling sensible heat flux using TSEB. Irrig. Sci., 37, 315–331. https://doi.org/10.1007/s00271-018-0611-y, 2019.

Norman, J.M., Kustas, W.P., and Humes, K.S.: Source approach for estimating soil and vegetation energy fluxes in observations of directional radiometric surface temperature, Agricultural and Forest Meteorology, 77, 263–293, 1995.

Pacheco-Labrador, J., El-Madany, T.S., Martín, M.P., Migliavacca, M., Rossini, M., Carrara, A., and Zarco-Tejada, P.J.: Spatio-Temporal Relationships between Optical Information and Carbon Fluxes in a Mediterranean Tree-Grass Ecosystem, Remote Sensing, 9, 608, https://doi.org/10.3390/rs9060608, 2017.

Perez-Priego, O., El-Madany, T.S., Migliavacca, M., Kowalski, A.S., Jung, M., Carrara, A., Kolle, O., Martín, M.P., Pacheco-Labrador, J., Moreno, G., and Reichstein, M.: Evaluation of eddy covariance latent heat fluxes with independent lysimeter and sapflow estimates in a Mediterranean savannah ecosystem, Agricultural and Forest Meteorology, 236, 87–99. https://doi.org/10.1016/j.agrformet.2017.01.009, 2017.

Perez-Priego, O., Katul, G., Reichstein, M., El-Madany, T.S., Ahrens, B., Carrara, A., Scanlon, T.M., and Migliavacca, M.: Partitioning eddy covariance water flux components using physiological and micrometeorological approaches, Journal of Geophysical Research: Biogeosciences, 2018.

Pianosi, F., Iwema, J., Rosolem, R., and Wagener, T.: A Multimethod Global Sensitivity Analysis Approach to Support the Calibration and Evaluation of Land Surface Models, Sensitivity Analysis In Earth Observation Modelling, Elsevier, 125–144, 2017.

Raupach, M.R.: Simplified expressions for vegetation roughness length and zero-plane displacement as functions of canopy height and area index, Boundary-Layer Meteorology, 71, 211–216, 1994.

Richardson, A.D., Keenan, T.F., Migliavacca, M., Ryu, Y., Sonnentag, O., and Toomey, M.: Climate change, phenology, and phenological control of vegetation feedbacks to the climate system, Agricultural and Forest Meteorology, 169, 156–173, https://doi.org/10.1016/j.agrformet.2012.09.012, 2013.

Rosolem R., Gupta H. V., Shuttleworth W. J., Zeng X., and Gonçalves L. G. G.: A fully multiple-criteria implementation of the Sobol′ method for parameter sensitivity analysis., Journal of Geophysical Research: Atmospheres, 117, https://doi.org/10.1029/2011JD016355, 2012.

Saltelli, A., Annoni, P., Azzini, I., Campolongo, F., Ratto, M., and Tarantola, S.: Variance based sensitivity analysis of model output. Design and estimator for the total sensitivity index, Computer Physics Communications, 181, 259–270. https://doi.org/10.1016/j.cpc.2009.09.018, 2010.

Santanello, J.A., and Friedl, M.A.: Diurnal Covariation in Soil Heat Flux and Net Radiation. Journal of Applied Meteorology 42, 851–862, https://doi.org/10.1175/1520-0450(2003)042<0851:DCISHF>2.0.CO;2, 2003.

Sauer, T.J., and Norman, J.M.: Simulated canopy microclimate using estimated below-canopy soil surface transfer coefficients, Agricultural and forest meteorology, 75, 135–160, 1995.

Sauer, T.J., Norman, J.M., Tanner, C.B., and Wilson, T.B.: Measurement of heat and vapor transfer coefficients at the soil surface beneath a maize canopy using source plates, Agricultural and Forest Meteorology, 75, 161–189, 1995.

Schaudt, K.J., and Dickinson, R.E.: An approach to deriving roughness length and zero-plane displacement height from satellite data, prototyped with BOREAS data. Agricultural and Forest Meteorology, 104, 143–155, 2000.

Sobol′, I.M.: Global sensitivity indices for nonlinear mathematical models and their Monte Carlo estimates, Mathematics and Computers in Simulation, 55, 271–280, https://doi.org/10.1016/S0378-4754(00)00270-6, 2001.

Sobrino, J.A., Jiménez-Muñoz, J.C., Verhoef, W: Canopy directional emissivity: Comparison between models, Remote Sens. Environ., 99, 304–314, https://doi.org/10.1016/j.rse.2005.09.005, 2005

Song, X., Zhang, J., Zhan, C., Xuan, Y., Ye, M., and Xu, C.: Global sensitivity analysis in hydrological modeling: Review of concepts, methods, theoretical framework, and applications, Journal of Hydrology, 523, 739–757, https://doi.org/10.1016/j.jhydrol.2015.02.013, 2015.

Stoy, P.C., El-Madany, T., Fisher, J.B., Gentine, P., Gerken, T., Good, S.P., Liu, S., Miralles, D.G., Perez-Priego, O., Skaggs, T.H., Wohlfahrt, G., Anderson, R. G., Jung, M., Maes, W. H., Mammarella, I., Mauder, M., Migliavacca, M., Nelson, J. A., Poyatos, R., Reichstein, M., Scott, R. L., and Wolf, S. : Reviews and syntheses: Turning the challenges of partitioning ecosystem evaporation and transpiration into opportunities. Biogeosciences Discuss., https://doi.org/10.5194/bg-2019-85, in review, 2019.

Su, Z.: The Surface Energy Balance System (SEBS) for estimation of turbulent heat fluxes, Hydrol. Earth Syst. Sc., 6, 85–100, https://doi.org/10.5194/hess-6-85-2002, 2002

Timmermans, W.J., Kustas, W.P., Anderson, M.C., and French, A.N.: An intercomparison of the Surface Energy Balance Algorithm for Land (SEBAL) and the Two-Source Energy Balance (TSEB) modeling schemes, Remote Sens. Environ., 108, 369–384, https://doi.org/10.1016/j.rse.2006.11.028, 2007.

van Griensven, A., Meixner, T., Grunwald, S., Bishop, T., Diluzio, M., and Srinivasan, R.: A global sensitivity analysis tool for the parameters of multi-variable catchment models, Journal of Hydrology, 324, 10–23. https://doi.org/10.1016/j.jhydrol.2005.09.008, 2006.

Weligepolage, K., Gieske, A.S.M., van der Tol, C., Timmermans, J., and Su, Z.: Effect of sub-layer corrections on the roughness parameterization of a Douglas fir forest, Agricultural and forest meteorology, 162, 115–126, 2012.

Xu, T., Bateni, S.M., Margulis, S.A., Song, L., Liu, S., and Xu, Z.: Partitioning Evapotranspiration into Soil Evaporation and Canopy Transpiration via a Two-Source Variational Data Assimilation System, J. Hydrometeorol., 17, 2353–2370, https://doi.org/10.1175/JHM-D-15-0178.1, 2016.

Zhang, X., Trame, M., Lesko, L., and Schmidt, S.: Sobol Sensitivity Analysis: A Tool to Guide the Development and Evaluation of Systems Pharmacology Models, CPT: pharmacometrics & systems pharmacology, 4, 69–79. https://doi.org/10.1002/psp4.6, 2015.

Appendix A

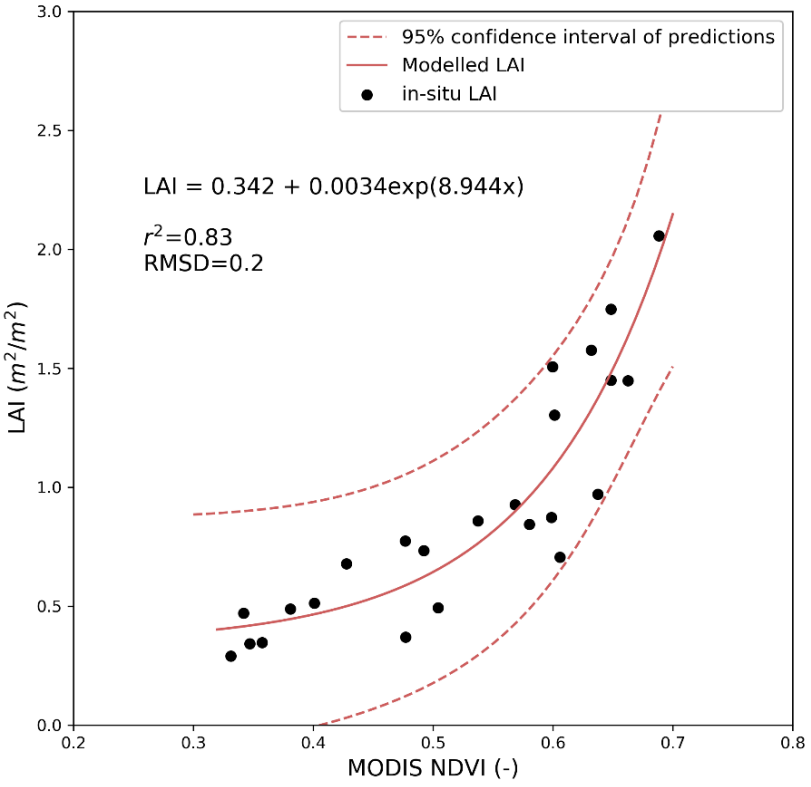

Figure A1. Empirical model between MODIS (MCD43A4) NDVI and in-situ destructive grass LAI measurements developed for Majadas experimental site.

895